

UC Berkeley

Research Reports

Title

Establishing Infrastructure Requirements for Bus Rapid Transportation Operations in Dedicated Bus Lanes

Permalink

<https://escholarship.org/uc/item/0xb67395>

Authors

Monismith, Carl L., P.E.
Weissman, Shmuel L., PhD
Popescu, Lorina
et al.

Publication Date

2008-11-01

CALIFORNIA PATH PROGRAM
INSTITUTE OF TRANSPORTATION STUDIES
UNIVERSITY OF CALIFORNIA, BERKELEY

Establishing Infrastructure Requirements for Bus Rapid Transportation Operations in Dedicated Bus Lanes

**Carl L. Monismith, Shmuel L. Weissman,
Lorina Popescu, Nicholas J. Santero**

**California PATH Research Report
UCB-ITS-PRR-2008-32**

This work was performed as part of the California PATH Program of the University of California, in cooperation with the State of California Business, Transportation, and Housing Agency, Department of Transportation, and the United States Department of Transportation, Federal Highway Administration.

The contents of this report reflect the views of the authors who are responsible for the facts and the accuracy of the data presented herein. The contents do not necessarily reflect the official views or policies of the State of California. This report does not constitute a standard, specification, or regulation.

Final Report for Task Order 6605

November 2008

ISSN 1055-1425

Establishing Infrastructure Requirements for Bus Rapid Transportation Operations in Dedicated Bus Lanes

Authors:

Carl L. Monismith, P.E., Director
University of California Pavement Research Center
Institute for Transportation Studies
University of California, Berkeley, California

Shmuel L. Weissman, Ph.D., President
Symplectic Engineering Corporation
Berkeley, California

Lorina Popescu, Engineer
University of California Pavement Research Center
Institute for Transportation Studies
University of California, Berkeley, California

Nicholas J. Santero, Associate Development Engineer
University of California Pavement Research Center
Institute for Transportation Studies
University of California, Davis, California

PREPARED FOR:

**Report to California PATH Program, University of California, Berkeley, in
cooperation with California Department of Transportation and Federal Highway
Administration, U.S. Department of Transportation**

Abstract

Bus Rapid Transit (BRT) has the potential to improve mass transit service and contribute to reduced traffic congestion in urban areas. To achieve this improvement in service BRT will require the use of dedicated bus lanes together with *lane assist and precision docking (LA/PD)* to accelerate the passenger boarding process. Using this approach, BRT lanes can be reduced somewhat in width. However, such a reduction will result in increased channelization of traffic which in turn can lead to a more rapid development of pavement distress. With today's improved pavement engineering technology, it is possible to design and construct pavement infrastructure which can result in long term and cost effective pavement performance (both in terms of pavement deterioration and equipment wear and tear). At the same time the system can be environmentally friendly with reduced traffic noise and increased passenger comfort from a smoother ride.

Keywords: Bus Rapid Transit, Pavement

TABLE OF CONTENTS

Introduction.....	7
Traffic Considerations	9
Structural Pavement Sections	10
Pavement Structural Section Analysis/Design.....	13
Construction Cost Estimates	17
Summary	18
References.....	19
Appendix A-1: AC Pavement Analysis/Design Methodology	21
Appendix A-2: Portland Cement Concrete (PCC) Pavement Analysis/Design Methodology	25
Appendix B: Construction cost Analyses	26
Appendix C: Establishing Infrastructure Requirements for Lane Assist/Precision Docking: Fatigue Analysis of Alternative Pavement Designs.....	27

LIST OF TABLES

Table 1: Bus Information	10
Table 2: Material Properties Used for the Pavement Analyses	14
Table 3: Material Unit Costs*	17
Table 4: Estimated Costs	17

LIST OF FIGURES

Figure 1: Proposed AC Transit Bus Rapid Transit Route (courtesy San Francisco Chronicle)....	8
Figure 2: Pavement cross sections considered for BRT lane (10 ft. wide); numbers in parentheses are layer thicknesses.....	12
Figure 3: Performance parameters used for the section thickness design.	14
Figure 4: Fatigue performance analysis system.....	15

INTRODUCTION

Bus Rapid Transit (BRT) has the potential to improve mass transit service and contribute to reduced traffic congestion in urban areas. To achieve this improvement in service BRT will require the use of dedicated bus lanes together with *lane assist and precision docking (LA/PD)* to accelerate the passenger boarding process. Using this approach, BRT lanes can be reduced somewhat in width. However, such a reduction will result in increased channelization of traffic which in turn can lead to a more rapid development of pavement distress. With today's improved pavement engineering technology, it is possible to design and construct pavement infrastructure which can result in long term and cost effective pavement performance (both in terms of pavement deterioration and equipment wear and tear). At the same time the system can be environmentally friendly with reduced traffic noise and increased passenger comfort from a smoother ride.

The study reported herein makes use of a specific example to illustrate the approach for a system proposed by Alameda/Contra Costa (AC) Transit District. This BRT is proposed to be developed along an Oakland/Berkeley/ San Leandro corridor which includes a dense residential area of approximately 360,000 people. Figure 1 illustrates the route. Three different pavement structures have been examined:

1. Flexible pavement (i.e., a pavement with asphalt concrete [AC] structural layers).
2. Rigid pavement (i.e., a pavement whose main structural element is a portland cement concrete [PCC] slab).
3. Pavement system consisting of two precast PCC beams located under the wheel paths as the main structural elements (with an infill of AC in the space between the two beams).

Each of the three pavements includes a special noise-reducing asphalt pavement surface system consisting of an asphalt-rubber binder (containing ground tire rubber particles) and a specially designed combination of aggregate particles. It is anticipated that this surfacing will be periodically replaced to insure continuous smoothness and noise reduction capabilities. The pavement sections have been designed to accommodate the total bus traffic estimated for a period of 50 years by the AC Transit Staff.

The following sections include: 1) summary of traffic estimates prepared by AC Transit Staff; 2) brief descriptions of the design approaches used for the three pavement structures; 3) initial cost estimates for the three pavement structures; 4) summary and recommendations; and 5) Appendices which include more detailed descriptions of the design methodologies for the AC and PCC pavements and the report prepared by Symplectic Engineering which describes a new approach to estimating cracking from repetitive trafficking in pavement materials. This was required to permit the design of the structure containing the precast beams to have comparable performance to the conventional concrete pavement.

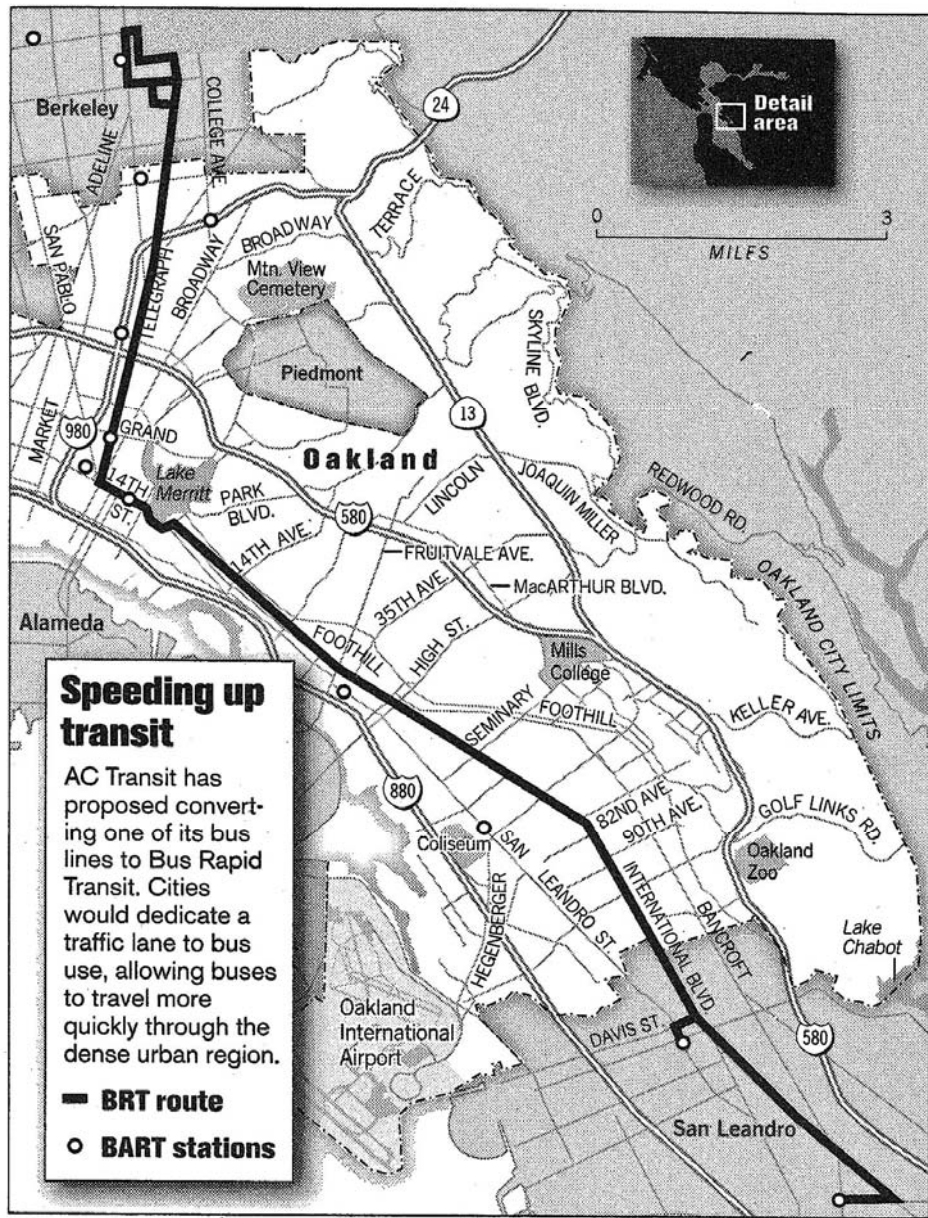


Figure 1: Proposed AC Transit Bus Rapid Transit Route (courtesy San Francisco Chronicle)

TRAFFIC CONSIDERATIONS

Estimates of bus traffic operations and bus technical data* were provided by AC Transit Staff. Table 1 contains information for the Rapid Transit (BRT 60 footer) and Regular (40 footer) buses.

The BRT operating plan (bus frequencies in year 2025) supplied by AC Transit are as follows:

Weekdays (253 per year)

Peak 8 hrs/day @ 3.6 min. headways (hr. starting: 6-9 AM, 3-6PM)

Base 7 hrs/day @ 5 min. headways (5AM, 10-2, 7PM)

Eve. 5 hrs/day @ 10 min. headways (8PM-midnight)

Owl 4 hrs/day @ 30 min. headways (1-4AM)

Sat./Sun./Holidays (112 per year)

Base 12hrs/day @ 7.5 min. headways (hr. starting: 7AM-6PM)

Eve. 7 hrs./day @ 10 min. headways (6AM, 7 PM-midnight)

Owl 5 hrs./day @ 30 min. headways (1AM-5AM)

Bus Routing

BRT-only bus lanes with guidance:

Telegraph Ave. from Bancroft in Berkeley to Shattuck Ave. in Oakland

Telegraph Ave. from 40th Street to 20th Street in Oakland

International/East 14th Street from 1st Ave. in Oakland to Davis Street in San Leandro

East 14th Street from Blossom Way to Bay Fair Drive in San Leandro

BRT shares lane with other buses without guidance:

Shattuck and Bancroft in Berkeley

Telegraph Ave. from Shattuck to 40th Street in Oakland

11th and 12th Streets between Broadway and oak in Oakland

BRT shares lane with mixed traffic and with other buses without guidance

20th Street and Broadway in downtown Oakland

12th Street between Oak and 1st Ave. in Oakland

East 14th Street between Davis and Blossom in San Leandro

In this study, the BRT pavements have been designed for 50 years, assuming that the 60 footer bus traffic estimated for 2025 is applied for this period. This estimate resulted in the following:

Repetitions of 15,600 lb. axles = 174,832 reps. per year x 50 years = 8.74×10^6

Repetitions of 26,500 lb. axles = 87,416 reps. per year x 50 year = 4.37×10^6

Structural pavement sections for the flexible (AC) and two rigid (PCC) pavements were designed to accommodate this traffic as will be seen subsequently.

*Van Hool Type AG 300 (60 ft. long) and Van Hool Type A 330 (40 ft. long); information can be found at the following Web site: www.vanhool.com.

Table 1: Bus Information

Bus Type	BRT 60 footer	Regular 40 footer
	Van Hool type AG-300 low-floor articulated bus, 60 ft. in length; 3 axles	Van Hool type A330 low-floor bus, 40 ft. in length; 2 axles
	Gross Axle Weight Rating, lb.	
Front axle	15,600 (2 tires)	15,600 (2 tires)
Middle axle	26,500 (4 tires)	-
Rear axle	15,600 (2 tires)	26,500 (4 tires)
Gross Vehicle Weight Rating	57,000	40,800

STRUCTURAL PAVEMENT SECTIONS

Three different structural pavement sections have been selected including two conventional pavements and a pavement section consisting of precast beams – one in each wheel path (similar to rails but significantly wider).

Flexible (AC) Pavement Section. The cross section for this pavement structure is shown in Figure 2a. The section consists of the following layers:

1. Open-graded AC with asphalt rubber binder, 2 in. thick. Its purpose is to provide a smooth wearing surface with tire/pavement noise somewhat less than conventional dense-graded AC. This will be replaced periodically (by milling and resurfacing)
2. Dense-graded AC containing a polymer modified asphalt binder (PG 64-28PM) 3 in. thick to provide a rut resistant layer for the channelized bus traffic.
3. Dense-graded AC containing conventional asphalt cement (PG 70-10). Its design thickness is based on the requirement (together with that of the next lower layer) that it provide adequate stiffness to the structural section to mitigate the potential for fatigue cracking in the AC from repeated trafficking. In addition, its thickness must be sufficient to insure that permanent deformations occurring in aggregate subbase and compacted subgrade will be minimal.
4. Rich-bottom AC layer containing the PG 70-10 asphalt with a binder content 0.5 percent (aggregate basis) greater than the AC in layer 3. The purpose of the increased binder content is to permit the mix to be compacted to higher degree of compaction (lower air void content) for improved fatigue and water resistance.
5. The untreated aggregate subbase serves as a working platform to insure that the succeeding layers of AC are properly compacted.
6. The subgrade soil, like the aggregate base, must be well compacted to minimize permanent deformation which could contribute to ruts at the pavement surface.

Rigid (PCC) Pavement Section. This pavement cross section is shown in Figure 2b and consists of the following layers:

1. Open-graded AC (OGAC) with asphalt rubber binder, 2 in. thick. Its function is the same as that the OGAC for the AC pavement section.
2. Jointed, plain concrete layer with dowels at transverse joints to provide sufficient stiffness to prevent fatigue cracking and reduce the potential for step faulting. The resultant faulting would contribute to an increase in the pavement roughness at the surface of the OGAC.
3. Dense-graded AC subbase provides a relatively plane surface on which to construct the PCC slab and mitigates the potential for pumping which can lead to deterioration of the PCC slab.
4. The untreated aggregate subbase serves the same function as for the AC pavement section.
5. The subgrade soil has the same requirements as for the AC pavement.

Precast PCC Pavement Section. This alternative pavement section consists of two precast PCC beams, each 50 in. wide as shown in Figure 2c. The AC mixes between the two beams provide lateral support as well as continuity of the surface between the two beams to support the OGAC surface course. The beams would be cast off-site and placed like rails. Dowels for load transfer would also be used at the joints in the beams. Like the other two pavements, the surface course consists of the OGAC and the underlying layers serve the same function as for the PCC section.

a. Flexible (AC) Pavement Section

Open-graded asphalt concrete, asphalt rubber (AR) binder (2 in.)	
Dense-graded asphalt concrete (AC) with polymer modified asphalt binder - Type A (3 in.)	Thick asphalt concrete layer
AC with conventional asphalt binder - Type A, (6 in.)	
Rich bottom AC, conventional binder with 0.5% increased binder content - Type A (3 in.)	
Untreated aggregate subbase (6 in.)	
Compacted subgrade	

b. Rigid (PCC) Pavement Section

Open-graded asphalt concrete, AR binder (2 in.)
Jointed PCC with dowels at transverse joints (10 in.)
Dense-graded asphalt concrete base - Type B (6 in.)
Untreated aggregate subbase (6 in.)
Compacted subgrade

c. Pavement Section with Precast PCC Beams in Wheelpaths

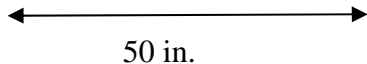
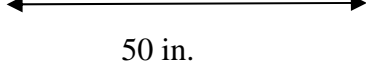
Open-graded asphalt concrete AR binder, (2 in.)		
Precast Concrete Beam (11 in.)  50 in.	Asphalt Concrete Type A (3 in.)	Precast Concrete Beam (11 in.)  50 in.
	Asphalt Concrete Type B (8 in.)	
Dense-graded asphalt concrete base, Type B, (6 in.)		
Untreated aggregate subbase (6 in.)		
Subgrade		

Figure 2: Pavement cross sections considered for BRT lane (10 ft. wide); numbers in parentheses are layer thicknesses.

PAVEMENT STRUCTURAL SECTION ANALYSIS/DESIGN

The design process for the three pavement sections required an initial selection of the pavement cross sections as shown in Figures 2a, 2b, and, 2c. For the AC section, Figure 2a, all of the layers, except layer 3 (DGAC with PG 70-10 binder) had predetermined thicknesses. The analysis/design process required determining a thickness of layer 3 which would permit the pavement to carry the total estimated BRT traffic for the design period with minimal fatigue cracking and surface rutting.

Similarly, for the conventional PCC pavement, Figure 2b, all thicknesses except the PCC slab were predetermined. Design considerations for the slab thickness included minimizing fatigue cracking and step faulting. For the precast beam section, all other layer thicknesses were set as was the 50 in. width of the beams to recognize the potential for a small amount of traffic wander. It was necessary only to determine the beam depth to minimize load associated fatigue cracking.

Flexible (AC) Pavement Section. The asphalt concrete pavement section was designed using a mechanistic-empirical approach. In this methodology the pavement is assumed to behave as a multilayer elastic system. With this assumption and the use of appropriate material properties, critical stresses/strains can be determined to estimate future performance.

For this type of pavement system, fatigue cracking initiating on the underside of the rich bottom layer and surface rutting which might result from deformations in the aggregate subbase and subgrade (Figure 2a) were the performance factors evaluated. Tensile strain on the underside of the rich bottom AC layer was considered the controlling parameter for fatigue cracking resulting from repeated bus loadings (1). Vertical compressive strain at the subgrade surface was used as the parameter to minimize rutting resulting from permanent deformations in the untreated materials. These parameters are shown schematically in Figure 3.

Relative to surface rutting, it is imperative that the AC mixes in layers 2 and 3 be properly designed to minimize their contribution to surface rutting. A Strategic Highway Research Program (SHRP) developed procedure has the capability to obtain suitable mixes for such pavements (2).

Material properties used for the analyses are listed in Table 2. The general framework for the fatigue analysis is illustrated in Figure 4. The more detailed procedure is described in Appendix A1. Results of the analyses indicate that structural pavement section can accommodate the anticipated bus loadings for period of 50 years.

Table 2: Material Properties Used for the Pavement Analyses

Layer	Material	Degree of compaction	Modulus, E psi	Poisson's ratio, ν
1	Open-graded AC	-	145,000 @ 20°C	0.3
2	Dense-graded AC layer, PG 64-28PM binder	$V_{air} = 6$ percent	145,000 @ 20°C	0.3
3	Dense-graded AC layer, PG 70-10 binder	$V_{air} = 6$ percent	1,000,000 @ 20°C	0.3
4	Dense-graded AC layer, PG 70-10 binder (+0.5% binder content)	$V_{air} \leq 3$ percent	1,000,000 @ 20°C	0.3
5	Aggregate subbase	100% of AASHTO T-180 max. dry density	8000 16,000	0.35 0.35
6	Subgrade	Upper 12 in., 95% of AASHTO T-180 max. dry density	4000 8000 15,000	0.4 0.4 0.35

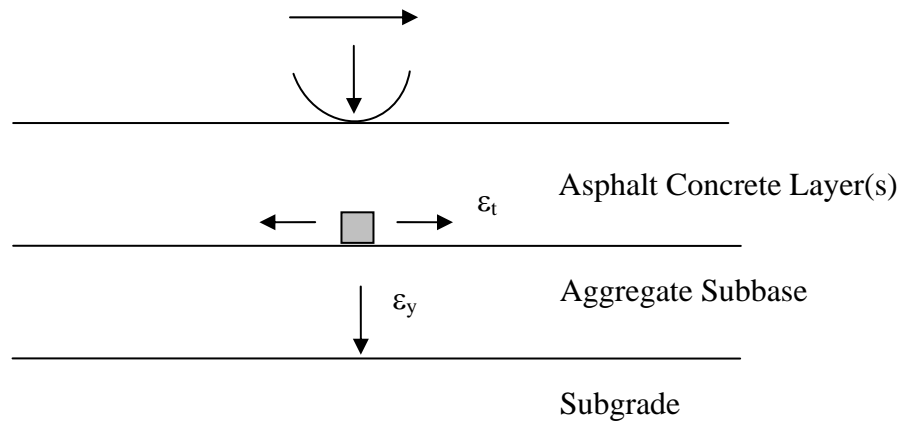


Figure 3: Performance parameters used for the section thickness design.

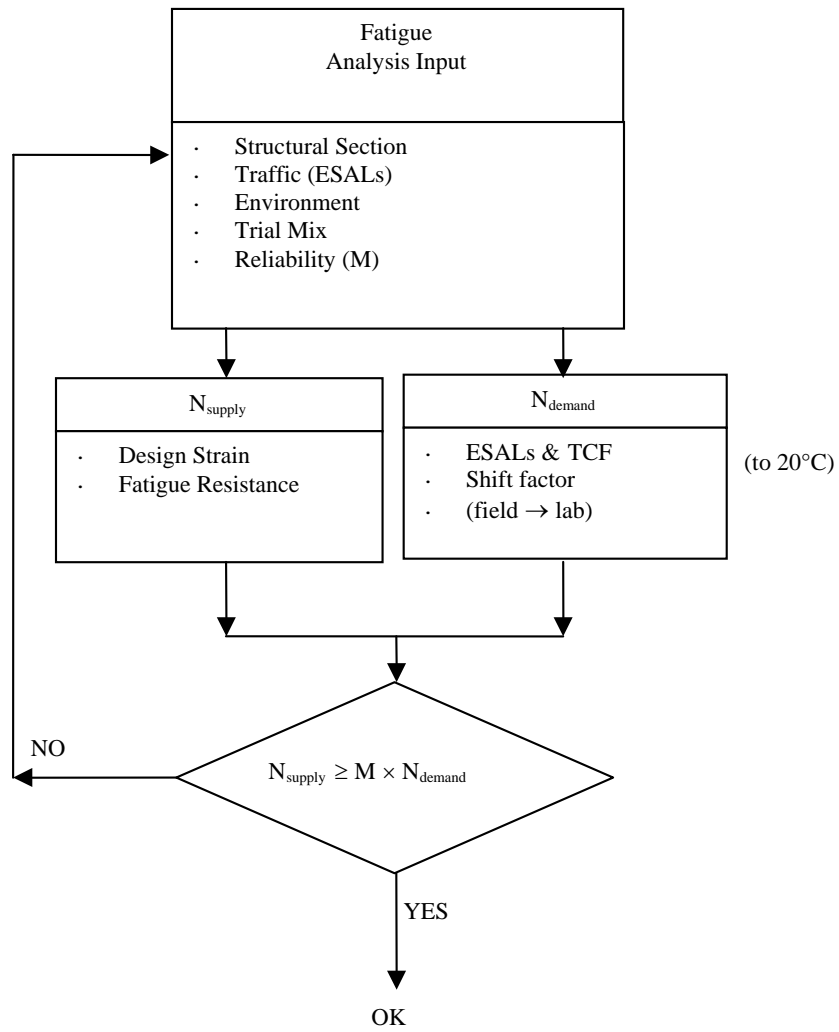


Figure 4: Fatigue performance analysis system.

Rigid (PCC) Pavement Section. The PCC structural pavement shown in Figure 2b was evaluated by the Portland Cement Association (PCA) structural section design procedure (3) for plain, jointed concrete pavements with dowels at the transverse joints (approximately 15 ft. spacing). This design procedure considers fatigue cracking in the concrete resulting from tensile stresses repeatedly applied and step faulting at transverse joints caused by repeated slab deflection, both from repeated trafficking.

The procedure includes provisions for asphalt concrete shoulders or tied concrete shoulders and transverse joints with and without dowel bars. The design section shown in Figure 2b was based on using the combination of doweled joints and asphalt concrete shoulders (likely the existing pavement).

This design was checked against the latest Caltrans design recommendations for PCC pavement thickness incorporated in the September 2006 of their Highway Design Manual (HDM), Chapter 620 (4). The required thickness of the PCC slab is 0.92 ft. (10.8 in.) according to the Caltrans recommendation in Tables 623.1D and 623.1E (representative of the environment in which this pavement). Thus by Caltrans standards the design would be considered slightly unconservative. Since a higher modulus of rupture was used for this design as compared to that generally used by Caltrans, the thickness resulting from the PCA procedure would appear reasonable. A more detailed discussion of this design methodology is included in Appendix A2.

For the design, the PCC modulus was assumed to 4,000,000 psi with a Poisson's ratio of 0.15. The modulus of subgrade reaction (the measure of support stiffness for the combination of AC base, aggregate subbase, and subgrade) was estimated to be 400 pci.

Precast PCC Pavement Section. No design procedure currently exists for the precast type of pavement structural system shown in Figure 2c. Accordingly, a damage law, based on continuum damage mechanics, was developed by the Symplectic Engineering Corporation to provide comparative behavior between a conventional concrete pavement and the pavement with the wide concrete beams. The results of this major effort are summarized in Appendix B.*

In the comparative analysis, the concrete slab thickness and the depth of the concrete beams were assumed to be the same (10 in.) for the analysis described in Appendix B.

The simulation results indicated a damage level about 6 percent larger for the beams versus the slab. Based on this analysis the beam depth was increased to 11 in. to obtain the same performance as the concrete slab.

*It should be noted that the methodology developed by Symplectic Engineering and described in Appendix B is essentially a new development to assess cracking in pavement structures.

CONSTRUCTION COST ESTIMATES

Cost estimates. Cost for the three pavement structural sections considered herein are based on cost data collected quarterly by Caltrans based on bid items obtained current construction contracts. The most recent version of the Caltrans costs summary “2007 Contract Cost Data: A Summary of Cost Items by Highway Construction Projects” has been used for the cost estimates. Information for average unit costs for PCC, open-graded asphalt rubber concrete (RHMA-O), dense-graded asphalt concrete (HMA-Types A and B), and aggregate base (AB). Unit costs for these materials are summarized in Table 3.

Table 3: Material Unit Costs*

Material	Unit Price (\$ per cu. yd.)
PCC	204.69
RHMA-O	185.65
HMA (Type A)	175.15
HMA (Type B)	174.49
AB (Class 2)	36.97

*Caltrans 2007 Contract Cost Data

Materials costs account for only a portion of the total costs. Mobilization, overhead, traffic control, earthwork, and other related items play a significant role in cost estimation. These elements, however, are not easily characterized by unit costs. Instead cost factors have been developed which relate material costs to total costs. Studies by staff of the UC Pavement Research Center have indicated that pavement materials account for about 42 percent of the total cost.

Appendix B contains the calculations in tabular form (Tables B1- B3) for the three pavement structural sections. Table 4 contains a summary of these costs, as well as the estimated total cost for each pavement structure.

Table 4: Estimated Costs

Pavement Structure	Materials	Total Cost
Flexible (AC) Pavement	\$438,200	\$1,043,000
Rigid (PCC) Pavement	\$600,800	\$1,431,000
Precast PCC Pavement	\$625,200	\$1,489,000

Other Considerations. Traditional agency costs, e.g. those shown in Tables 3 and 4 must often be combined other economic, construction (e.g. time limitations may preclude the use of certain materials), and environmental considerations. Road user costs, including time constraints, may influence the final decision as to which type of section might be constructed.

Depending on the type of cement selected and the time available for construction, PCC pavement sections may take longer to construct than HMA pavements due to extra critical path activities such as saw cutting and curing. Construction quality issues stem from onsite execution of the given structure’s design and specifications.

Both PCC and AC pavements require excellent construction control to insure long term performance. For example, for PCC pavements, control of the water/cement ratio must be maintained constant throughout the paving operation and curing conditions must be carefully controlled; HMA pavements require careful control of the degree of compaction to insure the requisite fatigue response and resistance to the effects of water and water vapor.

Precast PCC offers an alternative solution since the slabs are constructed off site in a controlled environment. Studies have shown that compared to on-site PCC, precast PCC structures reduce user costs due to the off site work. The amount of savings varies from project to project; limited experience, however, suggests that the reduction may be significant. Precast PCC also improves quality of the end product by allowing the concrete to be mixed, placed and cured in a controlled environment. To date, there is no research that compares the construction time and/or user costs of precast PCC to HMA,

SUMMARY

The purpose of this investigation has been to illustrate a methodology for designing the infrastructure necessary to accommodate special situations such as BRT lanes or dedicated truck lanes. The methodology not only provides the ability to effectively use pavement materials required for traffic operations for long term pavement performance but also to consider reduced lane widths for special circumstances such as the BRT lanes which include vehicle guidance. This methodology also has the ability to recognize the effects of the additional “wear” that can occur due to channelized traffic.

While the design capabilities currently exist to produce improved performing pavement structures, it must be recognized that carefully controlled construction practices are required to achieve the performance levels for which the design methodologies are capable.

It should be noted that a copy of the report was sent to the AC Transit Staff for comment; however, no comments were received. Because of this, it is likely that the report was not discussed with government officials and local businesses along the route. At the time of submittal of this report to AC Transit, the staff may have been meeting with these local groups because of differing views community views and the development of a anti-transit measure to be placed on the City of Berkeley’s ballot for November, 2008.

Finally, it should be noted that an effort was started in the study to develop an improved damage model for pavement materials subjected to repetitive traffic stressing. It is hoped that this promising approach, with only a limited application herein, might be continued. Such research would continue development to permit not only comparative performance of different systems but also develop realistic long term performance estimates for different pavement materials.

REFERENCES

1. Tayebali, A., J. A. Deacon, C. L. Monismith, J. S. Coplantz, J. T. Harvey and F. N. Finn. *Fatigue Response of Asphalt-Aggregate Mixes*. Report No. SHRP-A-404, Strategic Highway Research Program, National Research Council, Washington, D.C., 1994, 309 pp.
2. Sousa, J., J. A. Deacon, S. Weissman, J. T. Harvey, C. L. Monismith, R. B. Leahy, G. Paulsen and J. S. Coplantz. *Permanent Deformation Response of Asphalt-Aggregate Mixes*, Report No. SHRP-A-415. Strategic Highway Research Program, National Research Council, Washington, D.C., 1994.
3. Portland Cement Association. *Thickness Design for Concrete Highways and Street Pavements*, Skokie, IL, 1984, 46 pp.
4. California Department of Transportation (Caltrans), *Highway Design Manual*, Chapter 620, Sacramento, CA, September 2006.

APPENDIX A

A1. ASPHALT CONCRETE (AC) PAVEMENTS ANALYSIS/DESIGN METHODOLOGY

A2. PORTLAND CEMENT CONCRETE (PCP) PAVEMENT ANALYSIS/DESIGN METHODOLOGY

APPENDIX A-1: AC PAVEMENT ANALYSIS/DESIGN METHODOLOGY

This appendix contains some of the details of the analysis procedure used to determine an appropriate pavement structure for the AC pavement section.

Stiffness and Fatigue Equations for Modified and Conventional Binder Mixes

Table lists the regression equations of initial stiffness and fatigue for modified and conventional binder mixes.

Table A1. Regression equations of initial stiffness and fatigue life for modified and conventional binder mixes.

Modified Binder	
$E(\ln stif) = 9.1116 - 0.1137Temp$ (0.1493) (0.0071)	$R^2 = 0.93$
Conventional Asphalt	
$E(\ln stif) = 14.6459 - 0.1708AV - 0.8032AC - 0.0549Temp$ (0.6701) (0.0235) (0.1221) (0.0058)	$R^2 = 0.82$
$\ln nf = -30.819 - 5.3219 \ln stn$	NA

Where:

$\ln stif$ - natural logarithm of initial stiffness (MPa),

$\ln nf$ - natural logarithm of fatigue life,

$\ln stn$ - natural logarithm of tensile strain level,

AV - percent air-void content,

AC - asphalt content, percent

$Temp$ - temperature in C.

Note: The fatigue life equation for the mix containing the conventional binder was obtained at strain levels of 200 and 400 microstrain.

Traffic

1. Channelized traffic was assumed.
2. Trafficking was applied following time schedule supplied by AC Transit

Fatigue Analysis

Figure A1 illustrates the pavement structure and the associated loading configuration with the dual-tire configuration. Steps in the analysis are as follows:

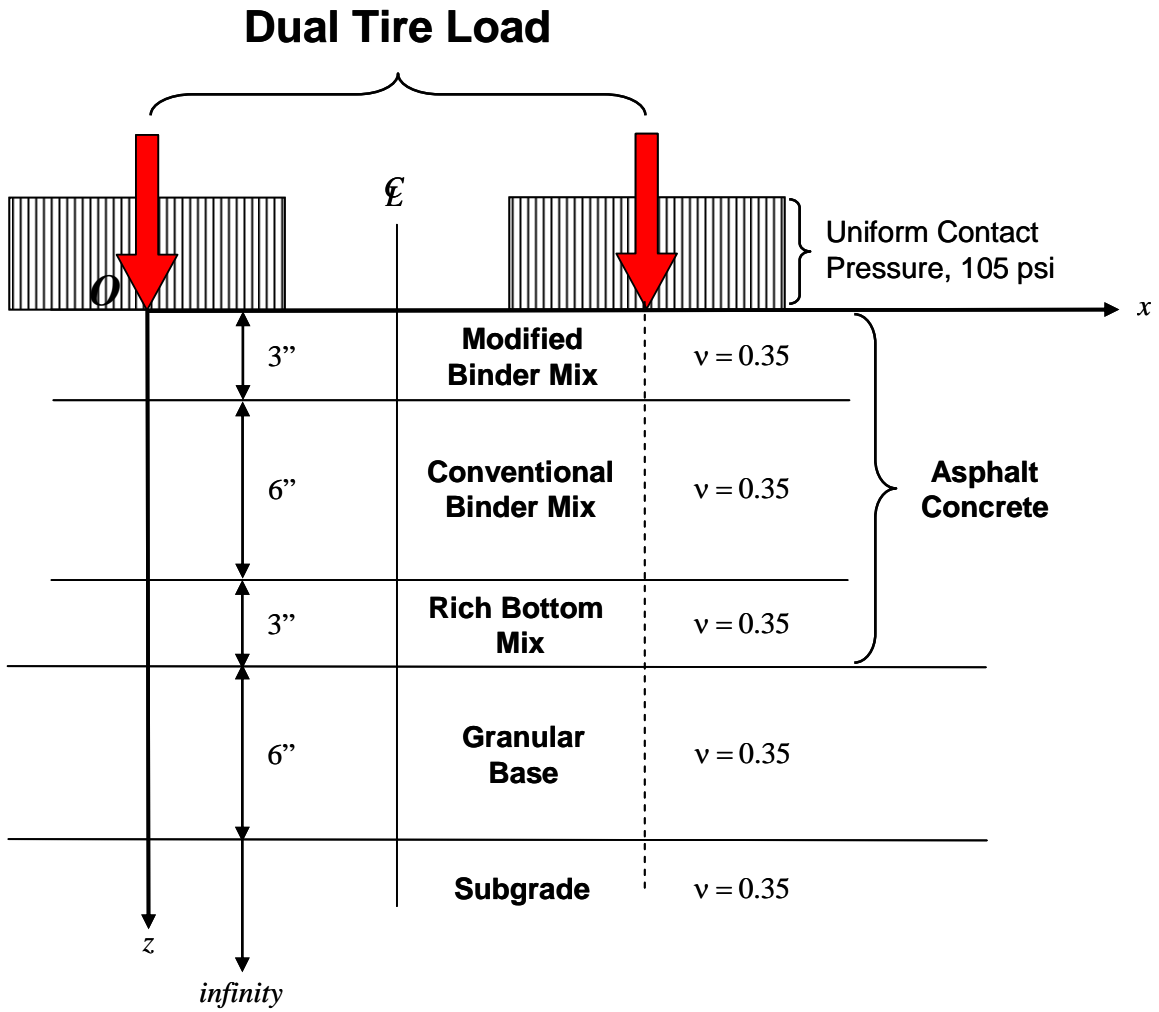


Figure A1. Schematic of AC structural pavement section.

1. Tensile strains were calculated at a depth of 12 in. and at a number of positions along the x -axis. The maximum tensile strain was then selected for the calculation of temperature equivalency factor (TEF) and temperature conversion factor (TCF).

2. Temperature data used in this calculation is based on the temperature data for Oakland, CA. Pavement temperature profiles, temperature gradients, temperatures at bottom of asphalt concrete were calculated on an hourly base for two year period 2004-2006. Temperature gradient is defined as $g\left(\frac{^{\circ}C}{in.}\right) = \frac{T_s(^{\circ}C) - T_b(^{\circ}C)}{12''}$, where T_s is the surface temperature and T_b the temperature at bottom of asphalt concrete.

The calculation of the temperature conversion factor is as follows:

1. obtain the laboratory fatigue life and initial stiffness equations,
2. run ELSYM5 to obtain the maximum tensile strain and then calculate the fatigue life,

3. calculate $TEF_i = \frac{N_f @ T_{ref} = 20C}{N_f @ T_i}$, and

4. $TCF = \sum_i^n f_i \cdot TEF_i$

3. The formulation for the shift factor calculation is $SF = 2.7639 \times 10^{-5} \cdot \epsilon^{-1.3586}$, where ϵ is the tensile strain. In this calculation, $N_f @ 20\text{ C}$ corresponds to the tensile strain which occurs at bottom of AC layer at 20C while subjected to a zero temperature gradient

4. The reliability multiplier M for a reliability level of 90 percent is determined from the following expression (in this case for a reliability of percent):

5. The allowable ESALs for the pavement design can then be calculated from the expression

$$ESAL_{allowable} = \frac{N_{f_{Lab}} \cdot SF}{TCF \cdot M}, \text{ where the } N_{f_{Lab}} \text{ is the laboratory fatigue life for the rich bottom layer at } 20C.$$

Permanent Deformation Analysis:

Subgrade Vertical Compressive Strain Analyses:

Vertical compressive strains at the subgrade surface were determined for the subgrade moduli shown in Table 2 in the body of the report.

Assumptions:

1. The surface permanent deformation is only attributed to the permanent deformation in the untreated layers
2. The Asphalt Institute subgrade strain criteria defined by the expression:
 $N = 1.05 \times 10^{-9} \cdot \epsilon_v^{-4.484}$ (Figure 3), were used for the analysis.
3. A cutoff point was set at 50×10^6 repetitions and 190 microstrain as shown in Figure . That is, it has been assumed that no rutting contributions to surface rutting from the untreated materials would occur for vertical compressive strains less than about 190 microstrain.
4. Stiffness calculations based on the regression equations were deemed to be appropriate outside the temperature range used to develop the expressions.

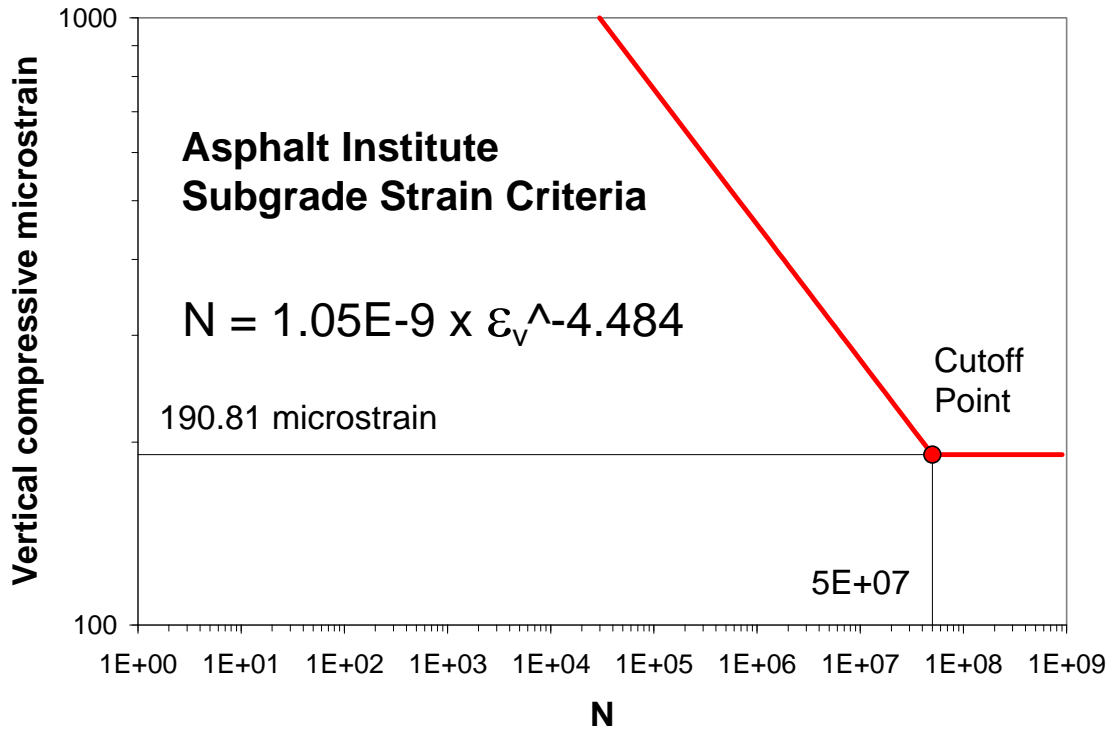


Figure A2. Asphalt Institute subgrade strain criteria.

The linear sum of cycle ratios cumulative damage hypothesis was used to establish an appropriate pavement thickness to insure minimal surface rutting (less than 0.5 in.) as follows using the laboratory initial stiffness regression equations:

5. Obtain the temperature profiles of the AC layer using the enhanced integrated climatic model (EICM),
6. Determine maximum vertical compressive strains at the subgrade surface on an hourly basis,
7. summarize the frequencies (f_i) of occurrence of maximum vertical compressive strains,

$$8. n_i = f_i \cdot ESAL_{Allowable}$$

$$9. N_i = 1.05 \times 10^{-9} \cdot (\varepsilon_v)_i^{-4.484}$$

$$10. \sum_i \frac{n_i}{N_i} = \sum_i \frac{f_i \cdot ESAL_{Allowable}}{N_i} = ESAL_{Allowable} \cdot \sum_i \frac{f_i}{N_i} = 1$$

$$\Rightarrow ESAL_{Allowable} = \frac{1}{\sum_i \frac{f_i}{N_i}}$$

11. If the $ESAL_{Allowable}$ are equal to or slightly larger than the estimated traffic, the total pavement section thickness is considered adequate.

APPENDIX A-2: PORTLAND CEMENT CONCRETE (PCC) PAVEMENT ANALYSIS/DESIGN METHODOLOGY

The methodology selected for the design of the PCC pavement is that developed by the Portland Cement Association (PCA). This design procedure includes consideration of fatigue cracking in the concrete slab and erosion at the joints. The fatigue analysis is included to insure that the slab thickness is sufficient to mitigate cracking from repeated trafficking. The purpose of the erosion analysis is to define a thickness that will control pumping and joint faulting. Input requirements for this analysis/design procedure include: 1) type of joint (with or without dowels) and shoulder (AC or tied PCC); 2) flexural strength of concrete, termed modulus of rupture (MR) at 28 days; 3) subgrade/subbase combined stiffness, termed modulus of subgrade reaction (k); 4) axle loads and repetitions associated with each axle load group expected during the design period (for this example only two).

Designs can be performed either using tables or graphs (“hand calculations or by use of the computer program PCAPAV. The design presented in this report was done using the tables and graphs contained in Reference (2). This procedure requires assuming a thickness of the concrete slab together with the input data listed above. For the assumed thickness both resistance to fatigue cracking and erosion are determined; the controlling thickness is governed by the more severe of the two distress modes. (For the thickness shown in Figure 2b, erosion control was the governing factor).

The analysis can be briefly summarized as follows:

1. For fatigue:

- a. Slab stresses are determined using the results of a finite element analysis program termed J Slab which determines stresses assuming that the slab behaves as a plate on a dense liquid subgrade whose stiffness is k.
- b. Use is made of a fatigue relationship established for portland cement concrete by the PCA with the following function format:
$$\log_e N = f(\text{load stress}/\text{MR})$$
- c. The linear sum of cycle ratios cumulative damage hypothesis is used to consider the effects of the different wheel load groups on fatigue cracking: This is the same approach as used for accumulating fatigue damage in the AC.

2. For erosion:

- a. A measure of erodability is determined from each axle load using an expression with the following functional format:

$$N = f\{([\text{slab corner deflection}] \times [\text{pressure at slab/foundation interface}]) / [\text{slab stiffness}/k]^{1/4}\}$$

- b. The linear sum of cycle ratios is computed for the various axle loads as in (c) above and the sum must equal or less than unity.

APPENDIX B: CONSTRUCTION COST ANALYSES

The following tables summarize the construction cost estimates for one lane 10 ft. wide and one mile long. These costs are based on the information contained in the main section of the report.

Table B1. Flexible (AC) Pavement Section

Layer	Material	Thickness (in)	Vol (yd ³)	Cost	Notes
1	RHMA-O	2	326	\$60,508	
2	HMA (type A)	3	489	\$85,630	PG 64-28
3a	HMA (type B)	6	978	\$170,613	PG 70-10
3b	HMA (type B)	3	489	\$85,306	+0.5% asphalt content
4	AB (class 2)	6	978	\$36,150	
Total Materials		20	3259	\$438,208	

Table B2. Rigid (PCC) Pavement Section

Layer	Material	Thickness (in)	Vol (yd ³)	Cost	Notes
1	RHMA-O	2	326	\$60,508	
2	PCC	10	1630	\$333,569	doweled JPCP, 15' joint spacing
3	HMA (type B)	6	978	\$170,613	PG 64-10
4	AB (class 2)	6	978	\$36,150	
Total Materials		24	3911	\$600,840	

Table B3. Precast (PCC) Pavement Section

Layer	Material	Thickness (in)	Vol (yd ³)	Cost	Notes
1	RHMA-O	2	326	\$60,508	
2a	Precast PCC	11	1494	\$305,771	Two 50 inch wide precast beams
2b	HMA (type A)	3	81	\$14,272	20 inch wide section
2c	HMA (type B)	8	217	\$37,914	20 inch wide section
3	HMA (type B)	6	978	\$170,613	
4	AB (class 2)	6	978	\$36,150	
Total Materials		25	4074	\$625,228	

**APPENDIX C: ESTABLISHING INFRASTRUCTURE REQUIREMENTS
FOR LANE ASSIST/PRECISION DOCKING: FATIGUE ANALYSIS OF
ALTERNATIVE PAVEMENT DESIGNS**

September 2007

Establishing Infrastructure Requirements for Lane Assist/Precision Docking: Fatigue Analysis of Alternative Pavement Designs

Project funded by
Caltrans, PATH Program
Task Order 6605
Pavement Research Center
Institute of Transportation Studies
University of California at Davis

Acknowledgment and Disclaimer

This work was performed as part of the California PATH Program of the University of California, in cooperation with the State of California, Business, Transportation, and Housing Agency, Department of Transportation; and the United States Department of Transportation, Federal Highway Administration.

This Final Report is in support of Task No. 6605 (Agreement No. SA5080) under Master Interagency Agreement No. 65A0208.



SYMPLECTIC
ENGINEERING CORPORATION

2901 Benvenue Ave., Berkeley, California 94705
telephone (510) 528-1251 • fax (510) 528-7102 • www.symplectic.com

ACKNOWLEDGMENTS

This project was sponsored by the California Department of Transportation, through the Regents of the University of California, under Interagency Agreement No. 65A0208, Task Order 6605. The Contract was awarded through the Institute for Transportation Studies at the University of California, Berkeley (University). Professor Carl L. Monismith served as Principal Investigator on the University side. We would like to acknowledge Professor Monismith's assistance, insights, and many discussions, which facilitated the work described in this report.

We would also like to acknowledge the many conversations we held with Dr. Rongzong Wu, of the University of California, regarding modeling fatigue distress in pavements.

The Symplectic Engineering Corporation team consisted of Drs. Jerome L. Sackman, and Shmuel L. Weissman. The latter served as the principal investigator.

TABLE OF CONTENTS

7

Executive Summary	31
Introduction.....	33
Material model	34
NONLINEAR ELASTIC MODEL	34
DAMAGE LAW	36
STRESS AND ALGORITHMIC TANGENT	38
Cycle Skipping.....	39
Pavement Sections	40
FLEXIBLE (AC) SECTION	40
RIGID (PCC) SECTION	40
PCC-BEAM SECTION.....	41
MATERIAL PROPERTIES	42
Numerical Simulations.....	46
AC PAVEMENT SIMULATION	49
PCC PAVEMENT SIMULATION	51
PCC-BEAM PAVEMENT SIMULATION.....	53
Conclusion and Recommendations.....	56
References.....	58

EXECUTIVE SUMMARY

This report studies fatigue damage of three pavement structures: flexible (AC), rigid (PCC), and rigid beam. The third type refers to a pavement whose main structural elements are PCC beams located under the wheel paths. The analysis employs three-dimensional finite element models to represent the structures. The structures are subjected to a dead load due to self-weight, and to cyclic loading from articulated buses of the type employed by AC Transit. Each tire is represented as a moving circular pressure footprint with a uniform contact pressure of 110 psi.

An exponential continuum damage mechanics law is used to represent the behavior of the main structural elements (AR8000 AC and PCC). This model introduces a history-dependent damage threshold in order to capture the behavior of the materials at low levels of cyclic loading. This threshold is assumed to increase monotonically with increased damage.

It is not feasible to compute the millions of bus traversals that a well built pavement should sustain before it fails. Therefore, a cycle-jump procedure has been developed to enable accurate predictions without the need to compute each bus traversal. This cycle-jump procedure differs from the common methodology employed in pavement analysis, which introduces an explicit function that describes the damage evolution as a function of the number of cycles. One important advantage of the proposed approach is that it enables the analysis of complex load cycles. For example, in the current study, traversal of a single bus includes three different axles, each exerting a different load.

Properties for the AR8000 AC material were determined by matching the results of (displacement controlled) beams with three-point support loaded to four different maximum strain levels. Good matches are obtained for the three higher levels of strain. At the lowest level, a good match is obtained up to about 120,000 cycles. At that point, the model predicts a rapid deterioration, while actual test data shows that the tested specimen failed at about 3,000,000 cycles. It should be noted, however, that a very small change in the linear hardening of the threshold would cause the model to predict that the specimen would never fail. Alternatively, if the prescribed displacement were slightly reduced, then the model would predict an infinite fatigue life. Thus, the discrepancy between the model prediction and actual test results were deemed acceptable.

Unfortunately, no raw data was available for fatigue tests of PCC materials. The data reported in the literature summarizes the fatigue life as a function of stress ratio (applied stress normalized by the modulus of rupture). Therefore, the damage properties developed for AR8000 are used also for PCC, with the threshold properties reduced by a factor of ten in order to enable damage development. Due to this limitation the analyses of two structures employing PCC do not provide actual life prediction. Instead, they offer a performance comparison between the two structural systems. This information is very useful because, while there are established empirical procedures to determine the expected fatigue life for PCC pavements, no such procedures are available for pavements employing beams. Thus, the present work can bridge the knowledge gap in empirical procedures.

The simulation results show, for the PCC beam dimensions considered herein, a damage level

that is roughly 6% larger than that observed for a corresponding number of cycles when a full PCC layer is employed. This finding should be used to obtain a life prediction based on an empirical design procedure. Alternatively, the thickness of the beam can be changed from 10 inches to about 10.25 inches in order to ensure that the two sections yield the same service life.

The simulations for the flexible pavements show an expected service life of about 500,000 bus traversals. This prediction is obtained by extrapolating the maximum damage observed in the pavement, and it falls short of the expected service life predicted by (validated) empirical procedures. On the other hand, if the prediction is based on extrapolating the change in deflection under the front tire, then a life expectancy of about 2,000,000 cycles is anticipated. This latter prediction is in line with what can be expected based on empirical design. Thus, two lessons must be drawn from the results reported herein. First, while the simulations herein offer a realistic analysis, they do not account for all the nonlinear effects present in the actual system. Therefore, a comprehensive validation should be undertaken. Unfortunately, such a validation program cannot be accommodated within the limited scope of this study. Second, it is not possible to extrapolate directly from the maximum damage recorded to the service life of pavements. A better measure is offered by examining the deflection history, which offers a system evaluation rather than an evaluation of what takes place at a specific material point.

Recommendations for future work include:

- Enhance the damage threshold hardening law.
- Obtain damage properties for PCC.
- Rerun simulations of rigid pavements (both slab and beam).
- Develop calibration factors by comparing the simulation results with field experience (rigid and flexible pavements).
- Consider the effect of thermal joints (PCC pavements).

INTRODUCTION

Bus Rapid Transit (BRT) holds the promise of improving mass transit services and reducing traffic congestion in urban areas. To attract commuters to BRT, the service must be reliable. Achieving the desired degree of dependability hinges on the use of dedicated lanes. Unfortunately, dedicated lanes encroach on an already crowded space, which forces mass transportation authorities to resort to the use of right-of-way. Buses employing lane assist travel on prescribed lateral positions (*i.e.*, the traffic is channeled). Consequently, the width of the lane can be reduced, which lowers the required right-of-way. Thus, lane assist can help reduce public objections to dedicated bus lanes.

Channeled traffic, however, may lead to the development of accelerated distress in pavements. As a result, reliable operation of BRT systems may be compromised by (relatively) frequent pavement maintenance. This report evaluates the effect of channeled articulated bus traffic on the fatigue life of the following three pavement structures:

1. Flexible pavement (*i.e.*, a pavement with Asphalt Concrete (AC) structural layers).
2. Rigid pavement (*i.e.*, a pavement whose main structural element is a Portland Cement Concrete (PCC) layer).
3. Rigid beam pavement (*i.e.*, a pavement with a PCC “beam,” located under the wheel path, as the main structural element).

The first two structures are representative of conventional pavements (*i.e.*, pavements where the structural layer extends throughout the section). The third structure is an unconventional pavement where, by taking advantage of the “channeled” traffic afforded by the use of lane assist technology, the main structural element is placed under the wheel path only. The PCC beams can be pre-fabricated offsite, transported to the site, and placed very quickly. This practice improves quality control, and reduces (on site) construction period.

This study employs three-dimensional finite element simulations to predict the fatigue life of pavements. Fatigue distress in the structural layers is represented by means of an exponential continuum damage mechanics law. This law introduces a threshold for damage, which has an initial value, and exhibits “linear hardening.”

A well-built pavement should support millions of bus traversals. Simulating each traversal is not computationally feasible. Therefore, a cycle-skipping procedure was developed. This procedure provides accurate predictions, while requiring only a fraction of the bus passes to be simulated. Unlike previous work reported in the literature (see *e.g.*, Wu [2005] and Peerlings *et al.* [2000]), the current extrapolation law does not introduce an explicit, *a priori* determined, function of the loading cycles. Thus, the model is based on first principles.

The remainder of this report is organized in five sections. First, the constitutive law is presented in Section 2. Second, the cycle-skipping procedure is provided in Section 3. Third, the pavement structures studied are described in Section 4. This section also provides damage properties that were back calculated from three-point beam flexure data. The results of numerical simulations are provided in Section 5. Finally, Section 6 offers conclusions and recommendations.

MATERIAL MODEL

This section contains a description of the constitutive model used herein to represent the different granular materials present in pavements. A key characteristic of these materials is that they exhibit markedly different properties in tension and compression. In the present model a nonlinear elastic law, described in Section 2.1, captures this feature. The focus of the present study is material degradation under high cycle loading (fatigue). In the present model this degradation is introduced via an isotropic damage law, which is presented in Section 2.2. The finite element computations shown in Section 5 require the formation of the stress and (algorithmic) tangent matrix, which are provided in Section 2.3.

NONLINEAR ELASTIC MODEL

A simple nonlinear elastic model is offered, which modifies the linear elastic law to account for pressure dependency of the shear and bulk moduli. Accordingly, the following strain energy function is introduced:

$$W := \frac{1}{2}KF_1(I_1)I_1^2 + 2\mu F_2(I_1)J_2 \quad (2.1)$$

In Equation (2.1) K and μ are the bulk and shear moduli, respectively; F_1 and F_2 are functions of the first strain invariant, $I_1 := \mathbf{1} : \boldsymbol{\varepsilon}$ ($\mathbf{1}$ is the second rank identity tensor); and $J_2 := \frac{1}{2} \mathbf{e} : \mathbf{e}$ is the second invariant of the deviatoric strain tensor, \mathbf{e} , which is given by:

$$\mathbf{e} := \boldsymbol{\varepsilon} - \frac{1}{3}I_1\mathbf{1} \quad (2.2)$$

Clearly linear elasticity is recovered by setting F_1 and F_2 to 1.

The stress arising from Equation (2.1) is given by:

$$\boldsymbol{\sigma} := \frac{\partial W}{\partial \boldsymbol{\varepsilon}} = \left(KF_1 I_1 + \frac{1}{2} KF_1' I_1^2 + 2\mu F_2' J_2 \right) \mathbf{1} + 2\mu F_2 \mathbf{e} \quad (2.3)$$

In Equation (2.3) $F_i' = \frac{dF_i}{dI_i}$ ($i = 1, 2$).

The tangent tensor is given by:

$$\mathbf{A} := \frac{\partial \boldsymbol{\sigma}}{\partial \boldsymbol{\varepsilon}} = \left(KF_1 + 2KF_1' I_1 + \frac{1}{2} KF_1'' I_1^2 + 2\mu F_2'' J_2 \right) \mathbf{1} \otimes \mathbf{1} + 2\mu F_2' (\mathbf{1} \otimes \mathbf{e} + \mathbf{e} \otimes \mathbf{1}) + 2\mu F_2 \mathbf{P} \quad (2.4)$$

In Equation (2.4) $F_i'' = \frac{d^2 F_i}{dI_i dI_i}$, and the (symmetric) fourth rank tensor \mathbf{P} is given by:

$$\mathbf{P} := \mathbf{I} - \frac{1}{3} \mathbf{1} \otimes \mathbf{1} \quad (2.5)$$

Note that the deviatoric strain tensor $\mathbf{e} = \mathbf{P}:\boldsymbol{\varepsilon}$.

Finally, to complete the description of the nonlinear elastic model, the functions F_1 and F_2 are defined as follows:

$$F_i := 1 - \frac{1}{\gamma_i} - \frac{2}{\pi\gamma_i} \text{atan}(\alpha_i [I_1 - \beta_i]) \quad (2.6)$$

Figure 2.1 provides a graphic representation of Equation (2.6). As can be seen these functions are monotonically decreasing, assuming the values of 1 at $I_1 = -\infty$ and $1 - \frac{2}{\gamma_i}$ at $I_1 = +\infty$.

Additionally, the value of α_i controls the sharpness of change, and the β_i controls the value of I_1 at which the transition occurs (*i.e.*, β_i is a shift along the I_1 axis). Thus, this function allows a smooth transition between the two asymptotic values for the shear and bulk moduli. It should be noted that based on physical grounds $\gamma_i \geq 2$ (*i.e.*, the shear and bulk moduli in tension are non-negative).

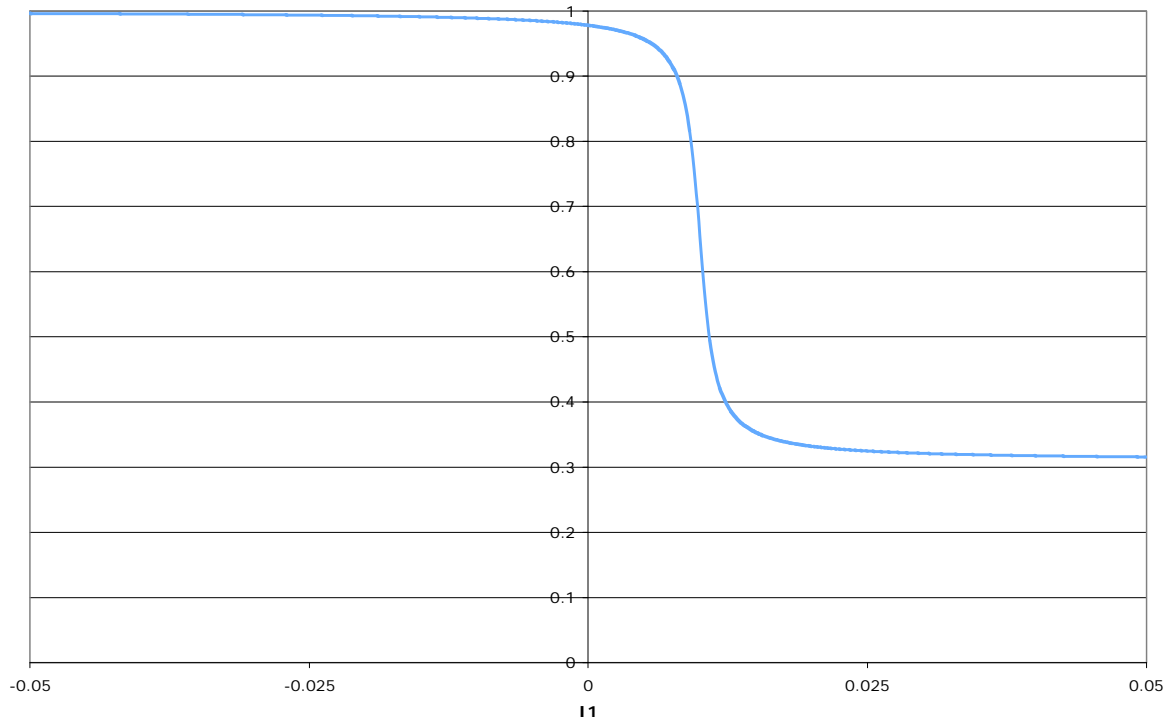


Figure 2.1: The dependence of F on I_1 ($\alpha = 1000$, $\beta = 0.01$, and $\gamma = 2.9$).

DAMAGE LAW

The objective of this study is to evaluate the degradation of pavements due to high cycle loading (fatigue). To this end the nonlinear elastic model described in Section 2.1 is enhanced to incorporate an isotropic continuum damage model (see *e.g.*, Lemaitre [1992] and references therein for a review of continuum damage mechanics). This section provides the details of this damage model.

Following continuum damage mechanics (see *e.g.*, Lemaitre [1992]) the point of departure for the proposed isotropic damage model is the assumption that the stress is given by:

$$\boldsymbol{\sigma} := (1-D) \frac{\partial W}{\partial \boldsymbol{\varepsilon}} \quad (2.7)$$

Comparing Equations (2.7) and (2.3) shows that the stress in the damaged continuum is reduced by a factor of $1-D$ relative to the undamaged continuum. To describe the damage model it is necessary to postulate an evolution equation and provide an initial value for D . In the present work the continuum is assumed to be initially undamaged so that the initial value for D is zero.

Let the eigenvalues of the strain tensor, $\boldsymbol{\varepsilon}$, be given by: λ_i ($i = 1, 2, 3$). The following norm is introduced:

$$\tilde{\lambda} := \sqrt{\langle \lambda_1 \rangle_1^2 + \langle \lambda_2 \rangle_1^2 + \langle \lambda_3 \rangle_1^2} \quad (2.8)$$

$\langle x \rangle_1 := \frac{1}{2}(x + |x|)$ in Equation (2.8) is the Macaulay bracket.

Next, a simple isotropic damage law is proposed so that Equation (2.7) takes the form:

$$\boldsymbol{\sigma} := \exp(-\delta_1 q_1) \frac{\partial W}{\partial \boldsymbol{\varepsilon}} \quad (2.9)$$

In Equation (2.9) δ_1 is a material parameter, and q_1 is an internal variable that is endowed with the following evolution equation:

$$\dot{q}_1 = \frac{\delta_2}{\delta_3} \frac{d}{dt} \left(\exp\langle \delta_3 \bar{\lambda} \rangle_1 \right) \quad (2.10)$$

The initial value for q_1 is given by: $q_1|_{\text{time}=0} = 0$ (this corresponds to the assumption that initially $D = 0$). In Equation (2.10) δ_2 and δ_3 are material properties, and $\bar{\lambda}$ is defined by:

$$\bar{\lambda} := \tilde{\lambda} - q_2 \quad (2.11)$$

q_2 is a second internal variable, describing a threshold for the growth of the damage. The following evolution equation is postulated for q_2 :

$$\dot{q}_2 = \delta_4 \frac{d}{dt} G(\bar{\lambda}) \quad (2.12)$$

The initial value for q_2 is given by: $q_{2|_{\text{time}=0}} = \delta_5$; δ_4 and δ_5 are material parameters; and G is a function of $\bar{\lambda}$, which renders the evolution of q_2 dependent on the value of q_2 . In the present work the function G is given by:

$$G := -\exp\left(\left\langle -\delta_6 \bar{\lambda} \right\rangle_1\right) \quad (2.13)$$

δ_6 is a material parameter.

Remark: The evolution equations for q_1 and q_2 render the model rate independent. ♦

Updating the internal variables q_1 and q_2 requires the integration of the evolution Equations (2.10) and (2.12), respectively. The backward Euler scheme is employed to this end. Accordingly, the evolution of the internal variables is discretized by:

$$\begin{cases} q_{1_{n+1}} = q_{1_n} + \frac{\delta_2}{\delta_3} \left\{ \exp\left\langle \delta_3 \bar{\lambda}_{n+1} \right\rangle_1 - \exp\left\langle \delta_3 \bar{\lambda}_n \right\rangle_1 \right\} \\ q_{2_{n+1}} = q_{2_n} + \delta_4 \left\{ G(\bar{\lambda}_{n+1}) - G(\bar{\lambda}_n) \right\} \end{cases} \quad (2.14)$$

The numerical algorithm for solving Equations (2.14) assumes that the eigenvalues of the strain tensor are given. Accordingly, it is necessary to first solve the (implicit) Equation (2.14)₂. To this end Equation (2.14)₂ is recast into the form given by:

$$R_{2_{n+1}}^i := q_{2_{n+1}}^i - q_{2_n} - \delta_4 \left\{ G(\bar{\lambda}_{n+1}^i) - G(\bar{\lambda}_n) \right\} = 0 \quad (2.15)$$

In Equation (2.15) the superscript i denotes the (local) iteration. Employing a Newton iteration yields:

$$q_{2_{n+1}}^{i+1} = q_{2_{n+1}}^i - \frac{R_{2_{n+1}}^i}{1 + \delta_4 \frac{\partial G}{\partial q_2}} \quad (2.15)$$

For the specific choice of G given by Equation (2.13), the derivative $\frac{\partial G}{\partial q_2}$ appearing in Equation (2.15) is given by:

$$\frac{\partial G}{\partial q_2} = -\delta_6 \exp\left(\left\langle -\delta_6 \bar{\lambda} \right\rangle_1\right) \quad (2.16)$$

To complete the description of the damage model it is necessary to compute $q_{1_{n+1}}$. Fortunately, this is accomplished by a straight forward evaluation of Equation (2.14)₁.

STRESS AND ALGORITHMIC TANGENT

After computing the internal variables, it is necessary to compute the stress and the algorithmic tangent matrix.¹ The stress is computed by evaluating Equation (2.9), with \mathbf{W} given by Equation (2.1). By definition the algorithmic tangent is given by:

$$\mathbf{A}_{\text{alg}} := \frac{d\boldsymbol{\sigma}}{d\boldsymbol{\varepsilon}} = \exp(-\delta_1 q_1) \mathbf{A} - \delta_1 \boldsymbol{\sigma} \otimes \frac{\partial q_1}{\partial \boldsymbol{\varepsilon}} \quad (2.17)$$

In order to compute the last term in Equation (2.17) it is necessary to introduce a new tensor, similar to the right Cauchy-Green tensor, \mathbf{C} . Accordingly, let

$$\mathbf{C} := 2\boldsymbol{\varepsilon} + \mathbf{1} \quad (2.18)$$

Further, let the eigenvalues of \mathbf{C} be denoted by ξ_i ($i = 1, 2, 3$), the eigenvectors of \mathbf{C} be denoted by \mathbf{N}^i , and introduce an additional tensor \mathbf{M}^i that is defined by:

$$\mathbf{M}^i := \xi_i^{-2} \mathbf{N}^i \otimes \mathbf{N}^i \quad (\text{no sum on } i) \quad (2.19)$$

With the above definitions in hand, it is possible now to compute $\frac{\partial \tilde{\lambda}}{\partial \boldsymbol{\varepsilon}}$, which is given by:

$$\frac{\partial \tilde{\lambda}}{\partial \boldsymbol{\varepsilon}} = \frac{1}{\tilde{\lambda}} \left(\sum_{i=1}^3 \langle \lambda_i \rangle_1 \xi_i \mathbf{M}^i \right) \quad (2.20)$$

Next, the derivative $\frac{\partial q_2}{\partial \boldsymbol{\varepsilon}}$ is given by:

$$\frac{\partial q_2}{\partial \boldsymbol{\varepsilon}} = \frac{\delta_4}{1 + \delta_4 \frac{\partial \mathcal{G}}{\partial \tilde{\lambda}}} \frac{\partial \mathcal{G}}{\partial \tilde{\lambda}} \frac{\partial \tilde{\lambda}}{\partial \boldsymbol{\varepsilon}} = \frac{\delta_4}{\left(1 + \delta_4 \frac{\partial \mathcal{G}}{\partial \tilde{\lambda}}\right)^2} \frac{\partial \mathcal{G}}{\partial \tilde{\lambda}} \frac{\partial \tilde{\lambda}}{\partial \boldsymbol{\varepsilon}} \quad (2.21)$$

Finally, after regrouping terms, the algorithmic tangent is given by:

$$\mathbf{A}_{\text{alg}} = \exp(-\delta_1 q_1) \mathbf{A} - \phi \boldsymbol{\sigma} \otimes \sum_{i=1}^3 \left(\langle \lambda_i \rangle_1 \xi_i \mathbf{M}^i \right) \quad (2.22)$$

The constant ϕ in Equation (2.22) is given by:

$$\phi := \frac{\delta_1 \delta_2}{\tilde{\lambda}} \exp(\delta_3 \tilde{\lambda}) \left(1 + \delta_4 \frac{\partial \mathcal{G}}{\partial \tilde{\lambda}} \right)^{-1} \quad (2.23)$$

¹ The Algorithmic tangent is need for quasi-static computations, which is the typical approach in pavement analysis where inertia terms can be neglected. The use of the algorithmic tangent is critical to ensure a quadratic rate of convergence (*i.e.*, the use of tangent matrix reduces the computational effort).

CYCLE SKIPPING

In a well-built pavement fatigue distress becomes important only after millions of load applications. Therefore, simulating each and every tire pass is not computationally feasible, and a method to approximate the solution is required. An approach used in pavement engineering is to postulate the fatigue damage evolution as a function of the number of cycles (itself depending on the state of stress or strain). Examples of this approach are offered by the work of Wu [2005] and Peerlings *et al.* [2000]. While this approach offers a high degree of numerical efficiency, it departs from first principles. A practical example of the shortcoming of this approach is the need to assume a single repeated cyclic loading. However, not all loads are equal. Relevant to this study is the need to simulate articulated buses where the front, middle, and rear tires exert different loads.

In this work a damage model is derived from first principles (see Section 2), without any recourse to assumptions on the loading cycle. Therefore, a different procedure is required for cycle jumping, which does not depend on *a priori* knowledge of the damage evolution as a function of the load cycles. The approach adopted herein employs the following algorithm.

1. Mark the beginning of the cycle (*i.e.*, note the time).
2. Store the damage parameters at all material points (Gauss points in the context of finite elements).
3. Proceed with the solution stepping one time-step at a time until arriving at the (user defined) end of cycle.
4. At each material point compute the damage increment during the cycle (*i.e.*, the difference between the damage at the end of the cycle and that stored at the beginning of the cycle).
5. At each material point determine how many cycles can be skipped by comparing the (user defined) allowable damage fraction with the actual damage fraction, which is defined by:

$$\text{damage fraction} := \frac{\text{damage accumulated during last cycle}}{\text{total damage}}$$

6. The number of allowable cycle jumps is then taken as the minimum of all allowable jumps.
7. Project the damage at each point by multiplying the damage increment by the number of cycles skipped.
8. Resolve the solution at the end of the cycle jump while forcing the damage to remain constant.

For example, if at a material point the total damage accrued is 0.3, and the damage increment during the last cycle is 0.03. Then, the damage fraction at that point is 0.1. If the user allows a fraction of 0.25, then the number of cycles skips allowed at that point is 2.

PAVEMENT SECTIONS

Three pavement sections are considered in this report. The first two are conventional flexible (Section 4.1) and rigid (Section 4.2) designs. The third takes advantage of the channeled traffic to replace the conventional PCC slabs with PCC beams located under the wheel paths, as described in Section 4.3. The material properties employed are presented in Section 4.4

FLEXIBLE (AC) SECTION

Table 4.1 describes the geometry of the AC section. The materials are listed in the order they appear in the pavement top to bottom.

Table 4.1: Flexible Section

Layer	Thickness (inches)
OGAC	2
PBA-6A	3
AR8000	6
AR8000 RB	3
UTSB	6
Subgrade	infinite

RIGID (PCC) SECTION

Table 4.2 describes the geometry of the rigid section. The materials are listed in the order they appear in the pavement top to bottom.

Table 4.2: Flexible Section

Layer	Thickness (inches)
OGAC	2
PCC	10
AC Base	6
UTSB	8
Subgrade	infinite

PCC-BEAM SECTION

Table 4.3 describes the geometry of the section employing a PCC beam under the wheel paths. The materials are listed in the order they appear in the pavement top to bottom. The PCC beam is 49.54 inches wide, centered about the tires. The gap between the PCC beams is filled with OGAC, as is shown in Figure 4.1. The figure shown is generated from the finite element mesh, so that only a portion of the section is shown. In particular, a plane of symmetry is assumed on the right side, so that only half the beam width is shown. The load shown represents the left tire of a dual-tire configuration employed by articulated buses (middle axle).

Table 4.3: Flexible Section

Layer	Thickness (inches)
OGAC	2
PCC/OGAC	10
AC Base	6
UTSB	8
Subgrade	infinite

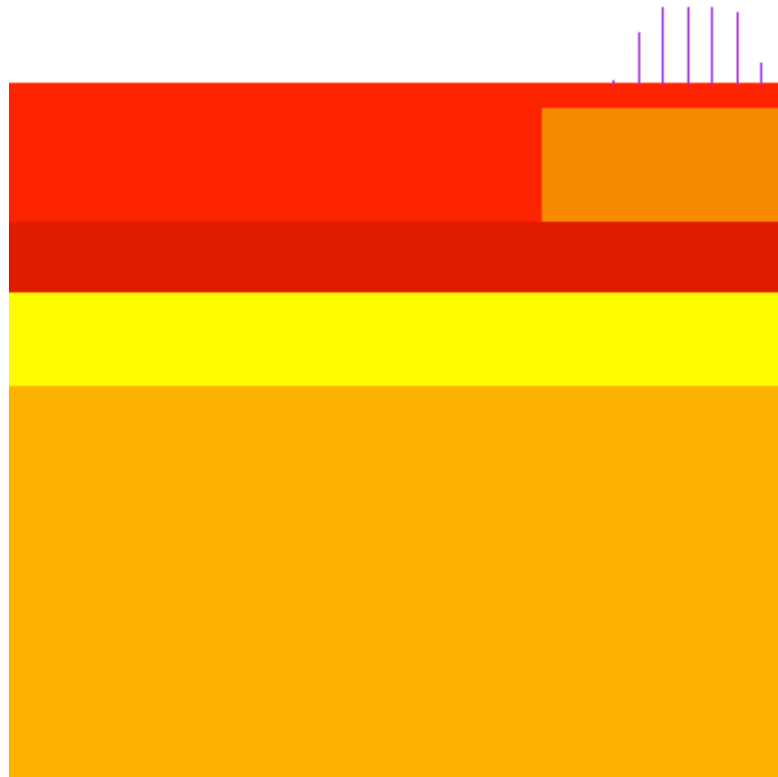


Figure 4.1: PCC-beam section. The orange rectangle under the load represents half the beam width. The load shown is the left of a dual-tire configuration (middle axle) of articulated buses.

MATERIAL PROPERTIES

All the pavement materials considered in this study are represented as nonlinear elastic media. Additionally, the structural layers (*i.e.*, AR8000, AR800 RB, and PCC) include the damage model. The properties used for the elastic model are summarized in Table 4.4. The same parameters are used for both F_1 and F_2 (see Equation (2.1)), which makes the two functions identical (*i.e.*, $F_1 = F_2$). This choice is imposed by limitations of the available data.

Table 4.4: Elastic Properties

Material	$\rho \left(\frac{\text{lb sec}}{\text{in}^4} \right)$	E (psi)	ν	K (psi)	G (psi)	α	β	γ
AC Base	2.173E-4	7.5E+5	0.3	6.250E+5	2.885E+5	1000	0	3.0
AR8000	2.173E-4	1.1E+6	0.3	9.167E+5	4.231E+5	1000	1.0E-4	2.9
AR8000 RB	2.173E-4	1.1E+6	0.3	9.167E+5	4.231E+5	1000	1.0E-4	2.9
PBA-6A	2.173E-4	1.0E+5	0.3	8.333E+4	3.846E+4	1000	0	5.0
PCC	2.173E-4	4.0E+6	0.2	2.222E+6	1.667E+6	1000	1.0E-4	2.9
OGAC	2.173E-4	1.5E+5	0.3	1.250E+5	5.769E+4	1000	0	3.0
Subgrade	1.798E-4	8.0E+3	0.4	1.333E+4	2.857E+3	1000	0	2.0
UTSB	1.948E-4	1.6E+4	0.35	1.778E+4	5.926E+3	1000	0	2.0

Mass density, ρ , is included in Table 4.4 in anticipation of incorporating the effect of self-weight in the simulations discussed in Section 5. Self-weight is important to the performance of the granular media, because it enhances their capability to sustain tension. For example, the subgrade material is assumed to possess very little ability to sustain tension (note that $\gamma = 2$ implies that the bulk and shear moduli assume an asymptotic value of zero as $I_1 \rightarrow \infty$).

The damage properties for AR8000 were extracted from a three-point fatigue beam testing provided by the Institute for Transportation studies at the University of California at Berkeley. This data is reported in Wu [2005]. The same properties are used for AR8000 RB as for AR8000. Tests were carried out at four different nominal strains: 20, 40, 60, and 80 micro-strains. Two replicas were tested at each strain level.

The material model described in Section 2 was used to approximate the test data. The identified properties are tabulated in Table 4.5. The fits obtained at the four strain levels are presented in Figures 4.2 through 4.5, which show the normalized applied force (*i.e.*, the applied force divided by the peak force applied in the first cycle) vs. the number of cycles. Two types of fit were obtained. First, a constant level of threshold was assumed (*i.e.*, $\delta_4 = 0$). This fit is labeled as Model-A. Second, the fits were obtained when the threshold is allowed to increase (harden).

These fits are labeled Model-B. All fits were obtained by solving a two-dimensional boundary value problem, approximated by a finite element model, representing the test setup.

Table 4.5: Damage parameters for AR8000 (and AR8000 RB)

Parameter	δ_1	δ_2	δ_3	δ_4	δ_5	δ_6
Model-A	1.0	0.65	0.65	0.0E+0	1.75E-4	0.0E+0
Model-B	1.0	0.65	0.65	6.0E-2	1.40E-4	6.0E-4

As can be seen the change in the threshold primarily affects the lower strain levels. Moreover, at the higher levels (60 and 80 micro-strains) the fit is very good. At lower levels the model under-predicts the life expectancy of the fatigue beam. This is most notable at 20 micro-strains, where the predicted life is about 120,000 cycles, whereas the actual is about 3,000,000 cycles (average of the two specimens). Here it is important to note the role played by the threshold. In particular, if the strain drops below the threshold, no damage occurs. As a result, if the simulation is repeated at a strain level below the 20 micro-strains, say 15 micro-strains, the model will predict that the beam will never fail. This, however, represents a shortcoming of the current model, and it should be remedied in future work. The addition of the “hardening” effect was intended to alleviate this problem. Indeed, as can be seen in Figure 4.2, the fit up to about 100,000 cycles matches the data quite well. However, the model enhancement did not significantly increase the range where the fit matched the data.

Data obtained for PCC provided charts showing the stress ratio vs. number of cycles to failure (see *e.g.*, Kohler *et al.* [2005]). To derive the damage parameters for the current model necessitates the data for each individual test (which is represented as a single point in the PCC charts). Therefore, the properties used herein for the PCC damage are based on those obtained for AR8000. Consequently, the fatigue life prediction is not reliable. Rather, conventional procedures should be used for this purpose. What is, however, of great importance is the ability to assess the performance of the section including PCC beams. The study in Section 5 provides the means to compare the performance of this design vs. the conventional rigid pavement design. Thus, actual prediction will be obtained using empirical procedures, and, for the PCC-beam section, using a conversion factor based on the study herein.

The threshold level used for the AR8000 would have resulted in no damage to the PCC pavement (note that the PCC layer is thicker than the AC layer, see Sections 4.1 through 4.3). Therefore, the threshold properties employed for PCC are reduced by an order of magnitude. The properties used for damage in PCC are tabulated in Table 4.6.

Table 4.6: Damage parameters for PCC.

Parameter	δ_1	δ_2	δ_3	δ_4	δ_5	δ_6
PCC	1.0	0.65	0.65	6.0E-2	1.40E-5	6.0E-5

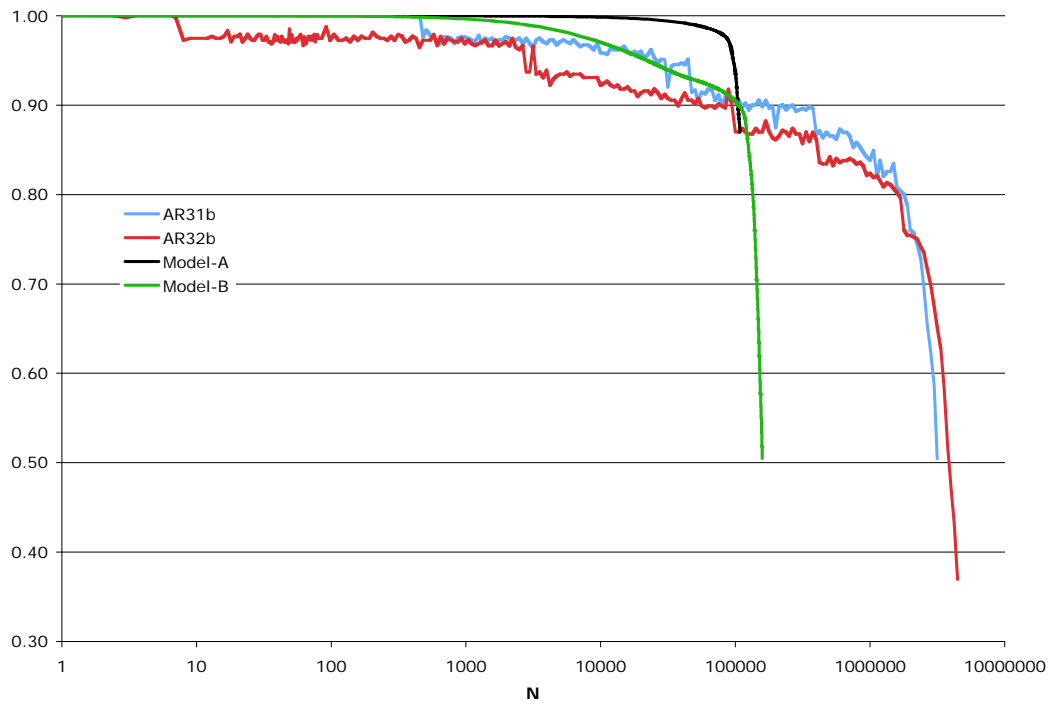


Figure 4.2: Fatigue beam test at 20 micro-strains, test data and model predictions.

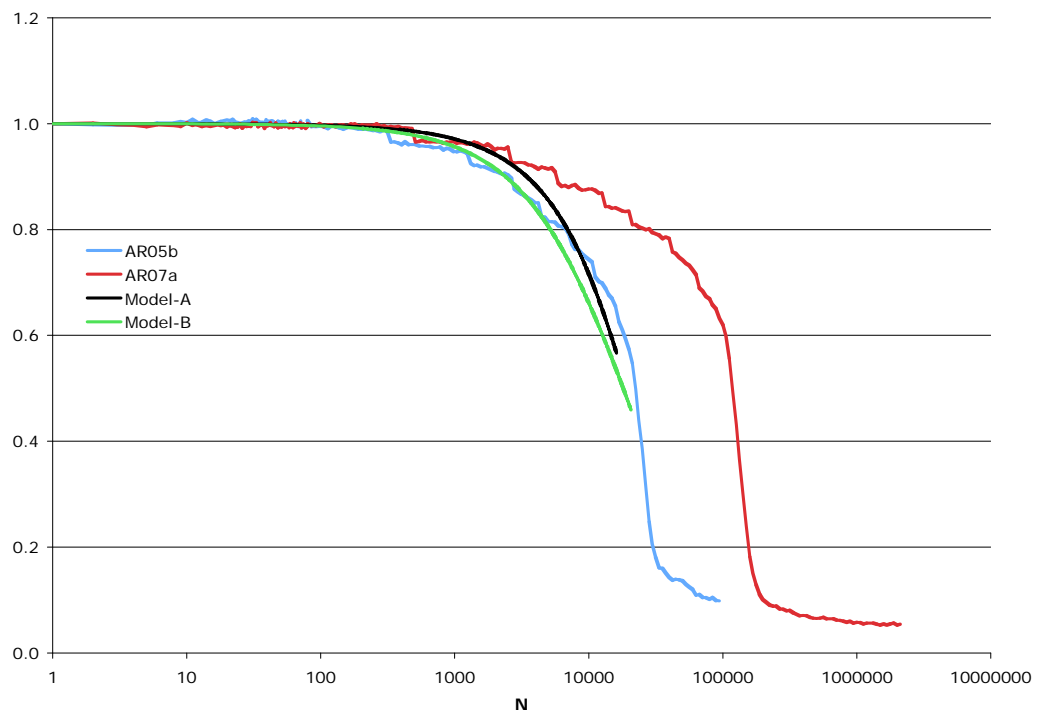


Figure 4.3: Fatigue beam test at 40 micro-strains, test data and model predictions.

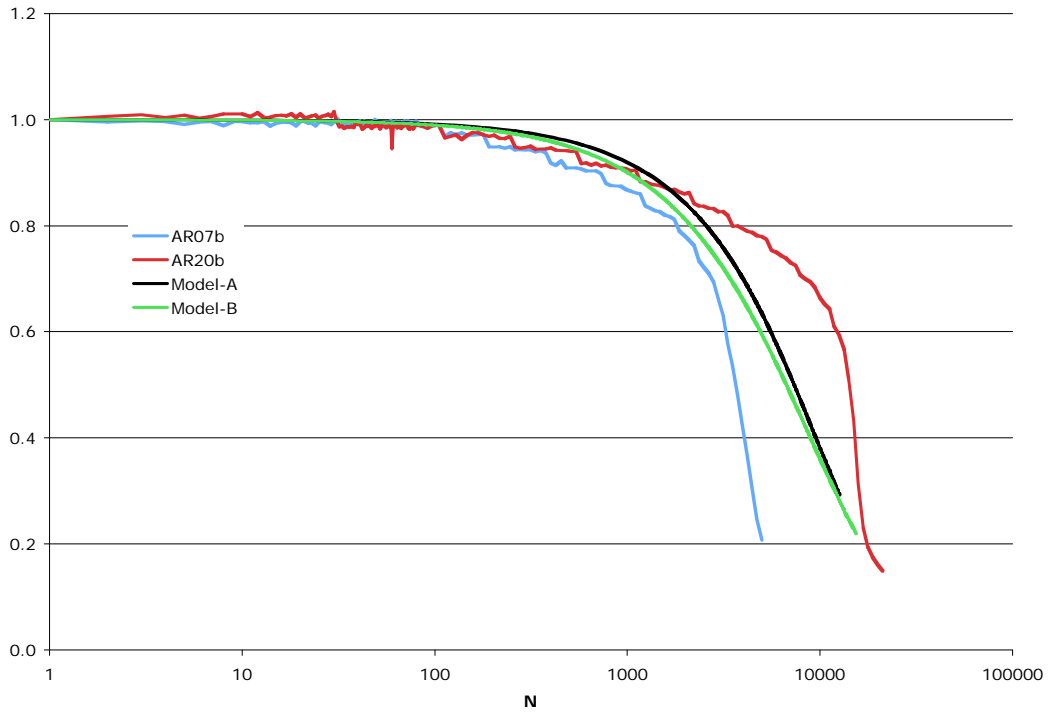


Figure 4.4: Fatigue beam test at 60 micro-strains, test data and model predictions.

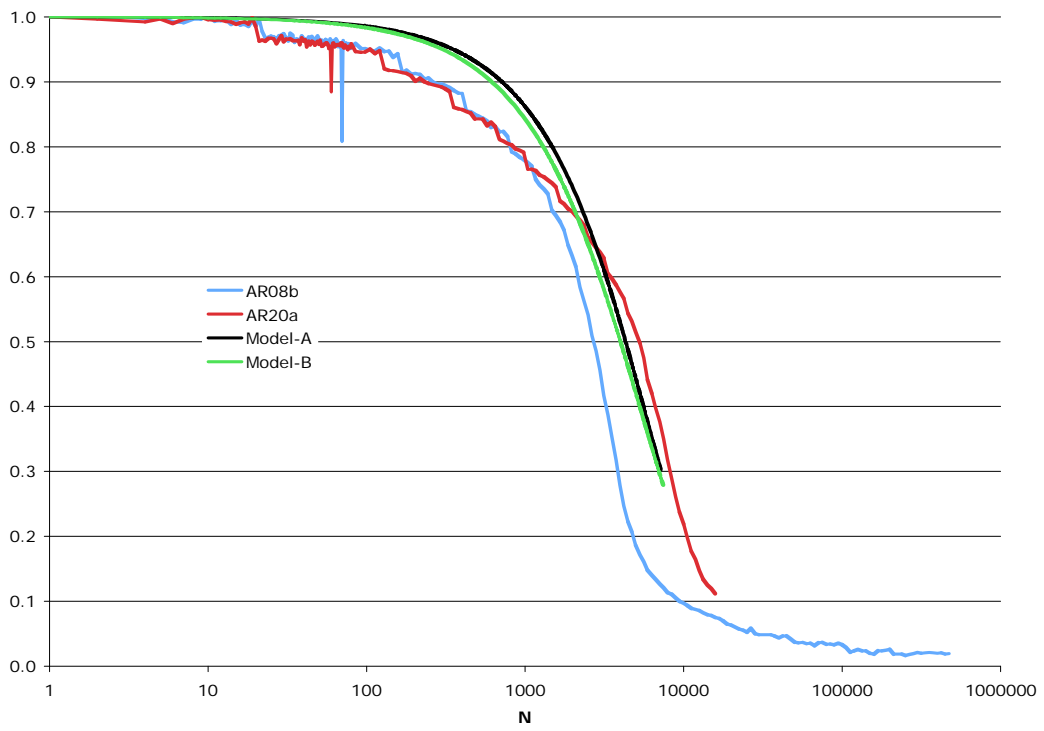


Figure 4.5: Fatigue beam test at 80 micro-strains, test data and model predictions.

NUMERICAL SIMULATIONS

This section provides the results of numerical simulations of fatigue damage to three pavement structures, which are described in Section 4. The loading consists of two components: a dead load due to self-weight, and moving loads associated with the wheels of articulated buses. These buses are equipped with three axles, as described in Table 5.1. All tires are represented as circular loads, assuming a uniform contact pressure distribution of 110 psi.

Table 5.1: Axle Loads

Axle	Load (pounds)	Number of tires
Front	15,600	2
Middle	26,500	4
Rear	15,600	2

All simulations in this section employ three-dimensional meshes. The analyses require the solution, at each time step, of 89,648 and 101,318 nonlinear equations for AC and PCC meshes, respectively. The portion of the pavement modeled is 96 inches wide and 192 inches long. The subgrade layer is assumed to extend only 60 inches deep, and to be supported by a rigid foundation. Figure 5.1 provides a perspective view of a typical mesh, and a top view (the mesh shown is the one used for the flexible pavement simulation). The top view clearly shows the refined zone in the area where tire loads are applied.

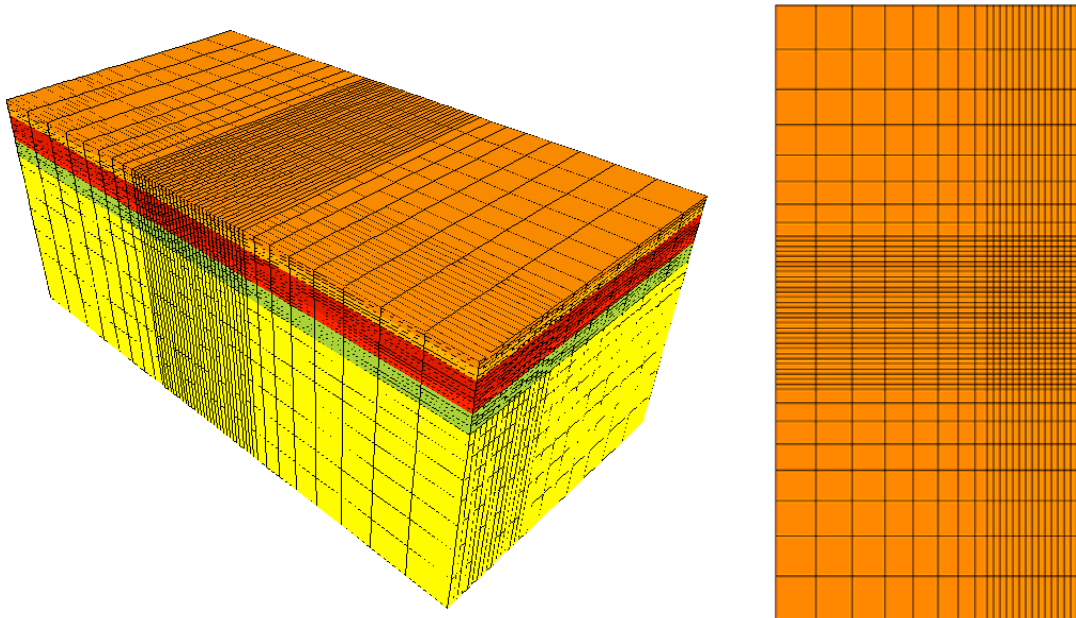


Figure 5.1: A sample mesh (perspective view (left), and top view (right)).

The following simplifying assumptions are introduced:

1. Inertia can be ignored, and the problem can be solved as quasi-static.
2. Interaction between the axles and interaction between tires on the left and right sides of the same axle can be ignored.
3. A symmetry condition can be applied in the (lateral) center of the tire configuration on each axle side (*i.e.*, if there is a single tire only half is modeled, and only one tire needs to be modeled in the case of a dual-tire configuration).
4. PCC slabs and beams can be assumed to be continuous (*i.e.*, thermal joints are ignored).
5. To minimize computations, each tire configuration is placed at a position located -2 radiuses from the (longitudinal) center of the mesh (*i.e.*, the center of the circular load is positioned at the said point). The tires are then moved in five equal steps to a position located +2 radiuses from the (longitudinal) center.
6. The load from only one axle is applied at any given time.
7. A load cycle consists of the passing of all three axles.

In reality, the loaded zone extends indefinitely in the direction of motion. Loading a strip of just six radii in length provided a first order approximation. More importantly, as shown in Figures 5.2, the discrete location of the loads results in a non-uniform damage in the longitudinal direction. Nevertheless, the analyses provide a reasonable approximation to the damage at the (longitudinal) center of the mesh.

A comparison of Figures 5.1b and 5.1c shows that the damage extends further, in the lateral direction, for PCC pavements. This is probably an artifact of the choice made for the damage threshold. This result should be revisited when proper damage properties for PCC are obtained.

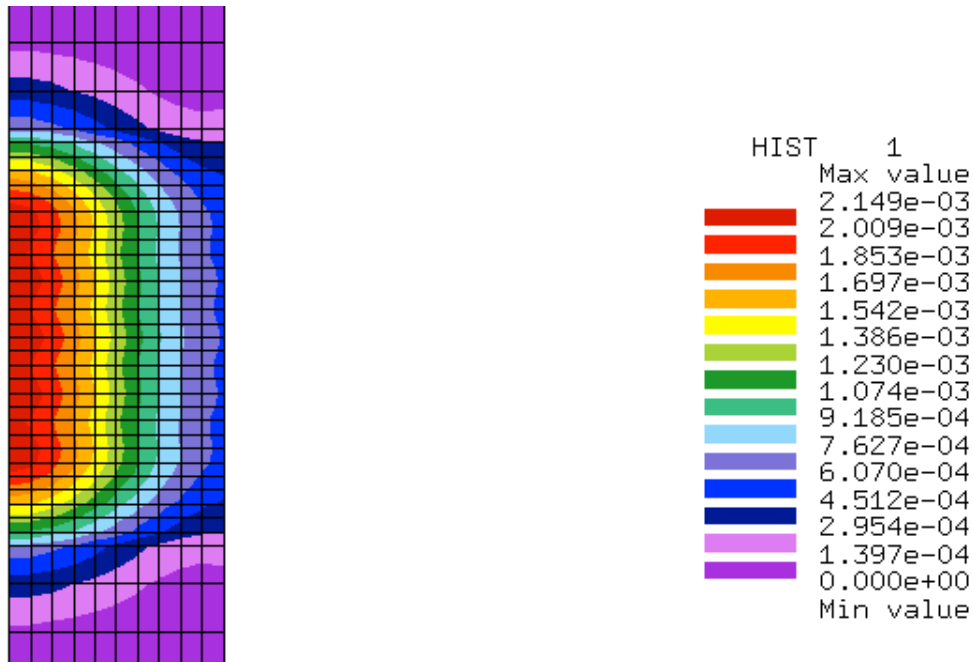


Figure 5.3a: Damage distribution on the bottom surface of the PCC beam after 38 cycles.

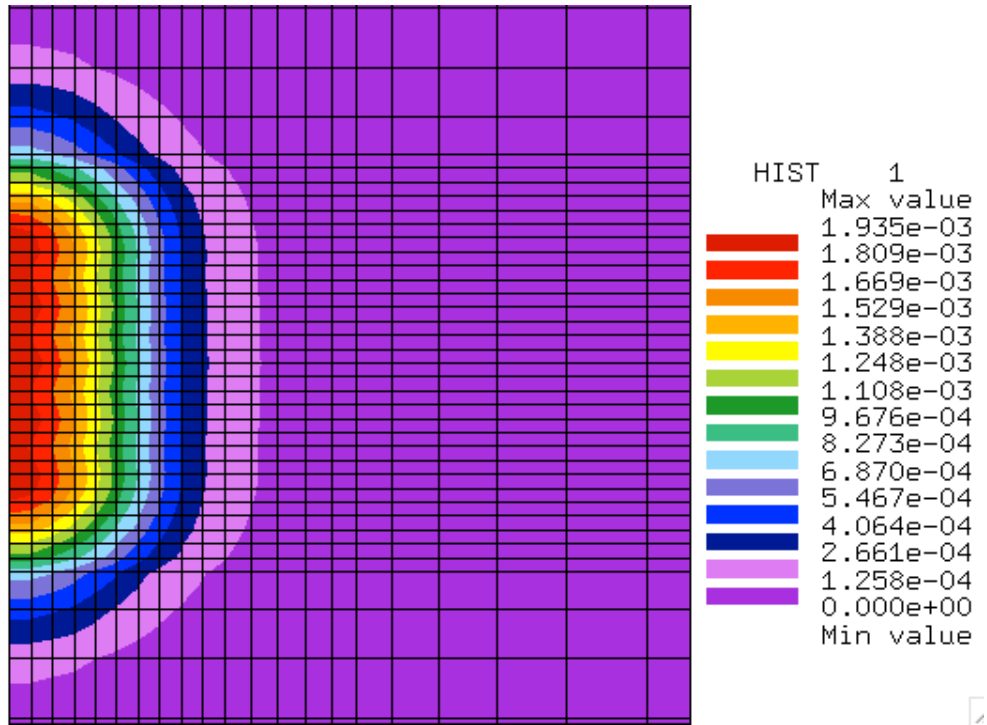


Figure 5.3b: Damage distribution on the bottom surface of the PCC layer after 36 cycles.

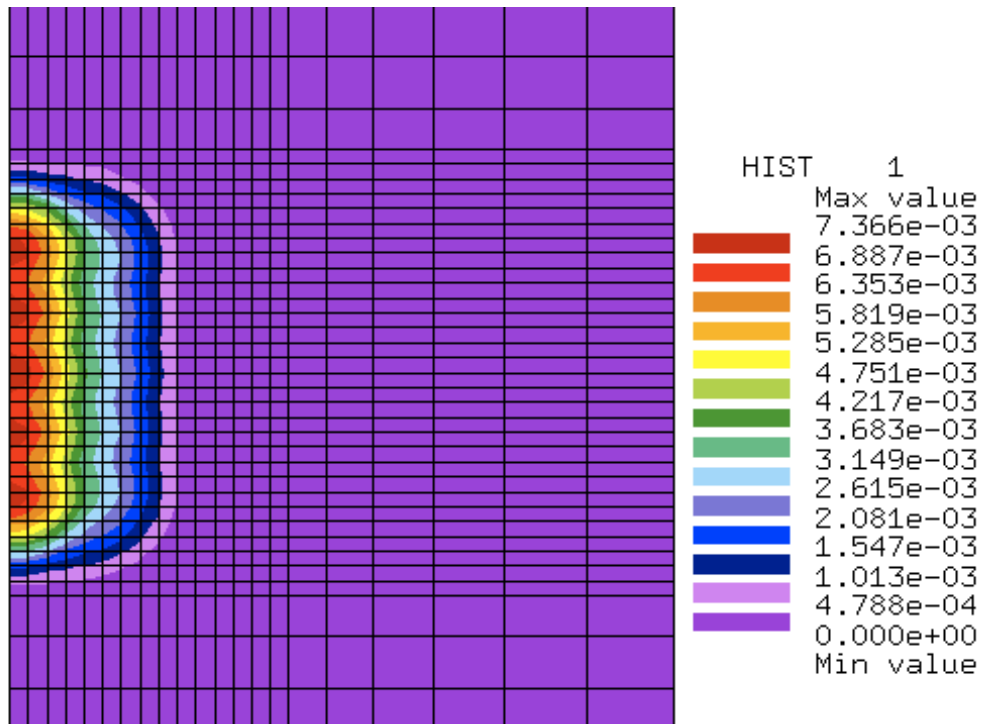


Figure 5.2c: Damage distribution on the bottom surface of the AR8000 RB layer after 60 cycles.

An important question is what measure should be used to assess the deterioration of the pavements with repeated loading. Two measures are used in this work. The first criterion is tracking the damage evolution at nodal points located at the bottom of the structural layer (*e.g.*, AR8000 RB for the flexible pavement, and PCC for the rigid pavements). Unfortunately, this criterion does not correspond to any measure used to assess the performance of real pavements. Therefore, a second criterion is introduced where the displacement under the front wheel is tracked. The second criterion integrates the effect of damage across the pavement to provide a measure of the pavement performance as a system, including the effect of damage accumulation on the performance of the pavement.

Note: Throughout this section damage and displacement histories are recorded at the time, within each cycle, when the front load is located above the (longitudinal) center of the pavement. ♦

The balance of this section is organized in three subsections. First, numerical results for the flexible pavement are provided in Section 5.1. Second, the results for the PCC section are given in section 5.2. Finally, the results for the PCC-beam section are presented in Section 5.3.

AC PAVEMENT SIMULATION

Figure 5.3 provides the history of the “stiffness reduction” (1-D) at nodal points located at the bottom of the AR8000 RB layer, labeled by the distance (in inches) from the (transverse) center of the mesh. The distribution of the damage along the transverse section (at the longitudinal center of the mesh) is shown in Figure 5.4. History of the normalized displacement under the front load is shown in Figure 5.5 (the displacement recorded at the first cycle is: 4.23231E-2 inches). The properties labeled as Model-B are used in this section for the AR8000 and AR8000 RB mixes.

The damage attains its maximum value at the (lateral) plane of symmetry of the load (labeled as $x = 0$). Extrapolating the final slope at $x = 0$ (Figure 5.3) suggests that a damage level of 50% can be expected at about one million cycles. It is also interesting to note that the damage is highly localized. At $x = 22$ the damage is reduced to zero (see Figure 5.4). This result supports assumption two above (ignoring the interaction between different axles and left and right sides of the same axle). Moreover, this result suggests that a 48 inches wide beam located under the tires could provide a good support for the wheels, without significant deterioration of the service life of the pavement.

The displacement under the front tire is used as a second gage to assess the deterioration of the pavement performance. A comparison of Figures 5.5 and 5.3 suggests that the degradation of pavement progresses slower than the damage evolution. For example, extrapolating the data in Figure 5.5 predicts that at the millionth cycle the displacement would increase by 10% (over the first cycle), whereas extrapolating Figure 5.3 suggests a damage level of 50% at the same number of cycles.

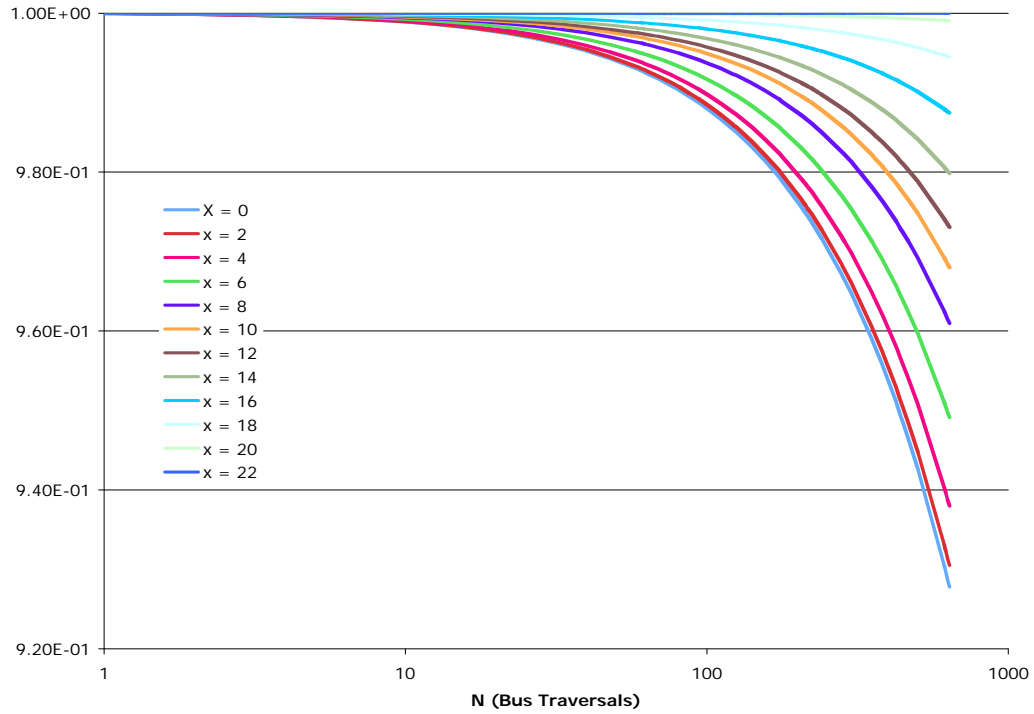


Figure 5.3: History of the residual stiffness (1-D) at various locations along a transverse section located at the (longitudinal) center of the mesh.

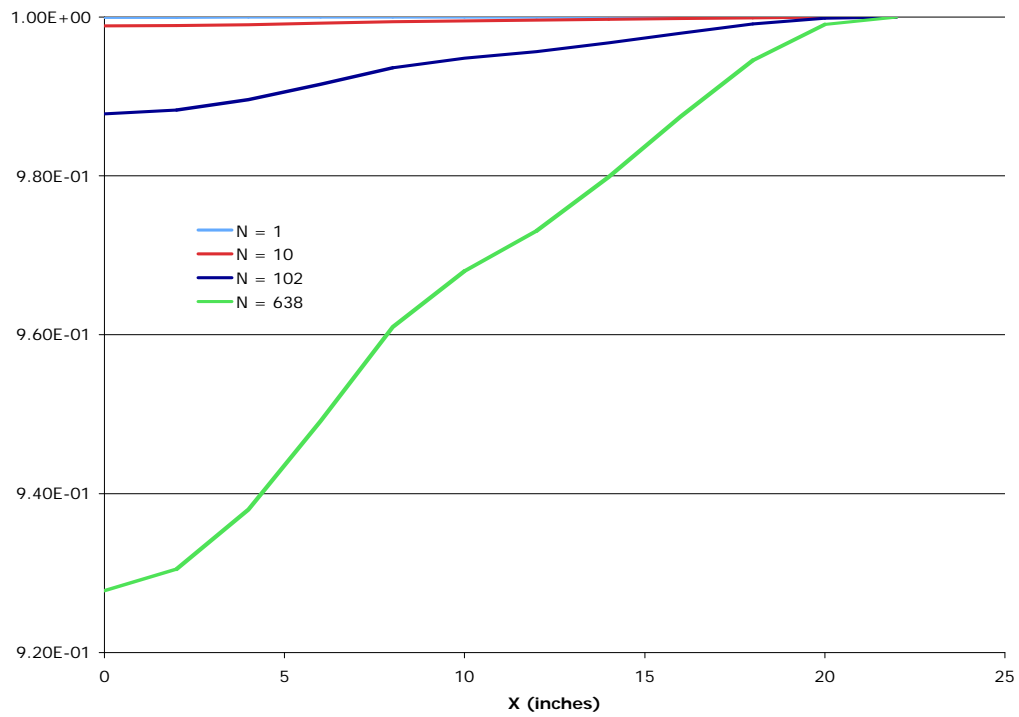


Figure 5.4: Distribution of residual stiffness along the transverse center of the mesh.

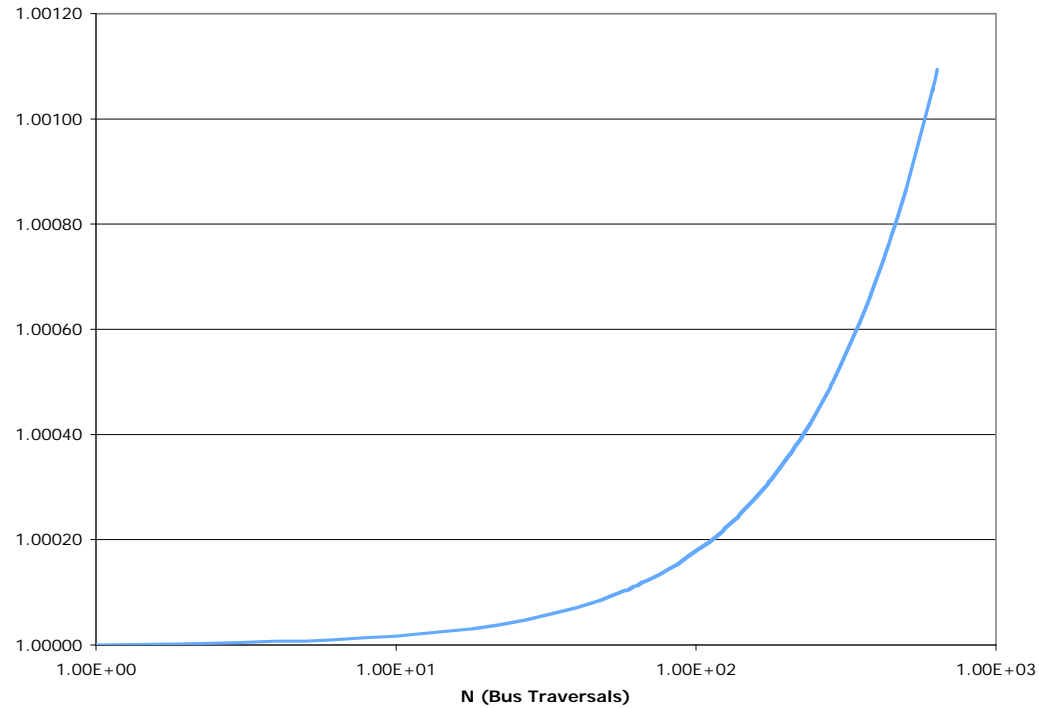


Figure 5.5: History of the (normalized) displacement under the front load.

PCC PAVEMENT SIMULATION

Figure 5.6 provides the history of the “stiffness reduction” (1-D) at nodal points located at the bottom of the PCC layer, labeled by the distance (in inches) from the (transverse) center of the mesh. The distribution of the damage along the transverse section (at the longitudinal center of the mesh) is shown in Figure 5.7. History of the normalized displacement under the front load is shown in Figure 5.8 (the displacement recorded at the first cycle is: 3.07658e-02 inches).

The maximal damage is recorded at the (lateral) plane of symmetry of the load (labeled as $x = 0$). Extrapolating the final slope of the damage at $x = 0$ (Figure 5.6) predicts that a 50% damage can be expected at about five million cycles.

Note that the damage extends further, in the lateral direction, than it does for the flexible pavement. This is because of the lowered threshold (see Table 4.6). This issue should be revisited after damage properties are obtained directly for the PCC material in a way analogous to that used to extract the properties for AR8000 AC mix.

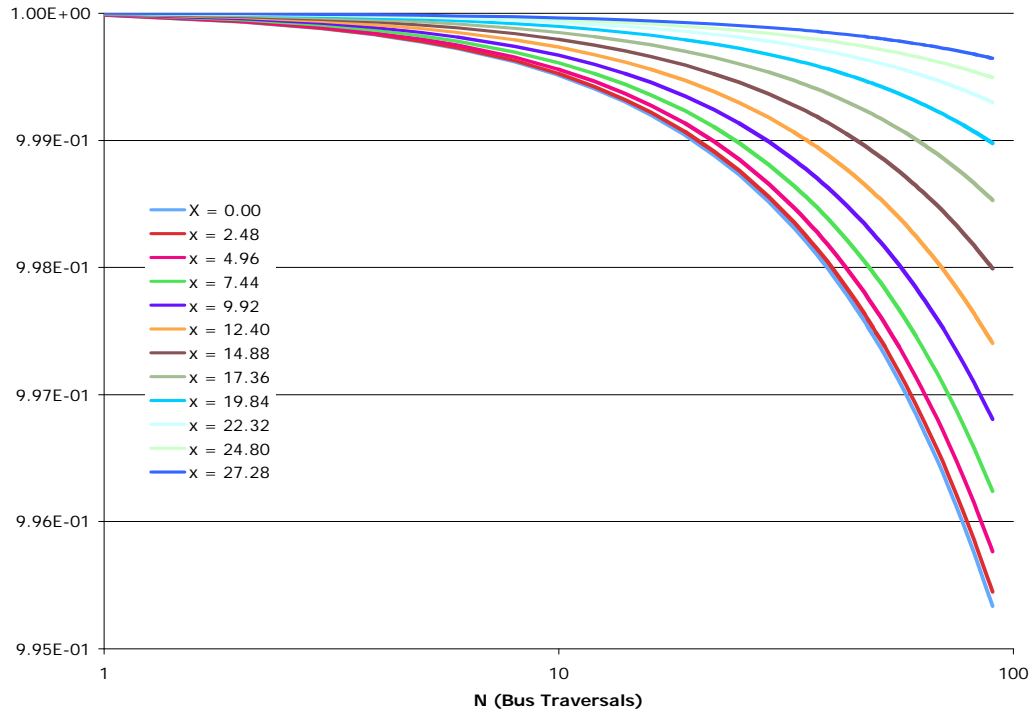


Figure 5.6: History of the residual stiffness (1-D) at various locations along a transverse section located at the (longitudinal) center of the mesh.

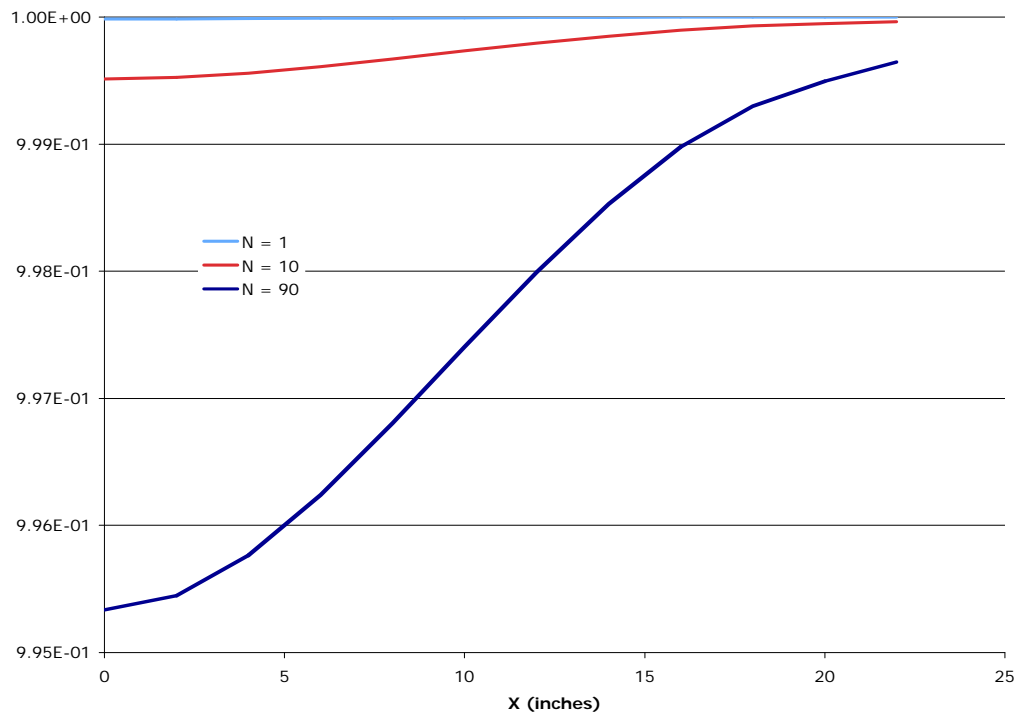


Figure 5.7: Distribution of residual stiffness along the transverse center of the mesh.

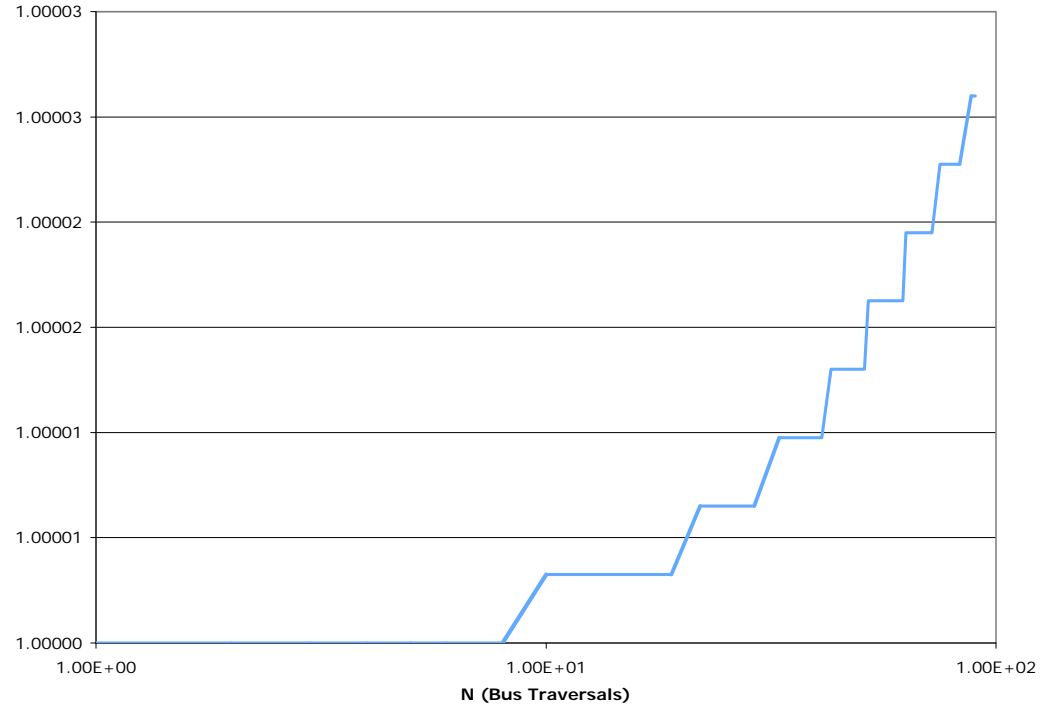


Figure 5.8: History of the (normalized) displacement under the front load.

PCC-BEAM PAVEMENT SIMULATION

Figure 5.9 provides the history of the “stiffness reduction” (1-D) at the bottom of the PCC beam, labeled by the distance (in inches) from the (transverse) center of the loading tires. The distribution of the damage along the transverse section (at the longitudinal center of the mesh) is shown in Figure 5.10. History of the normalized displacement under the front load is shown in Figure 5.11 (the displacement recorded at the first cycle is: 4.23231E-2 inches).

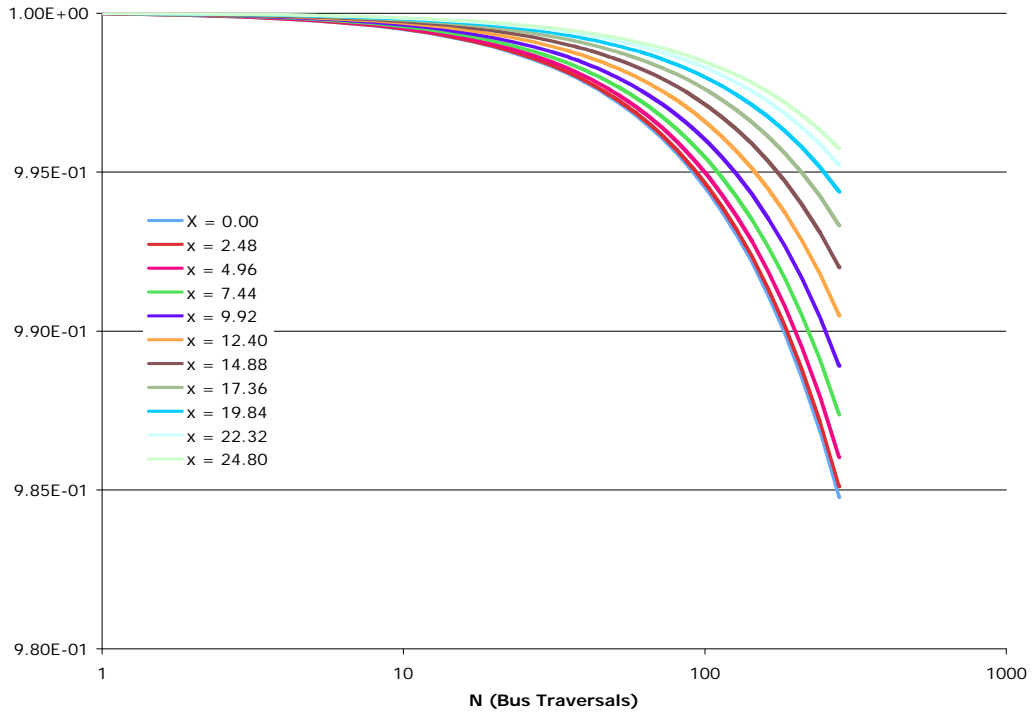


Figure 5.9: History of the residual stiffness (1-D) at various locations along a transverse section located at the (longitudinal) center of the mesh.

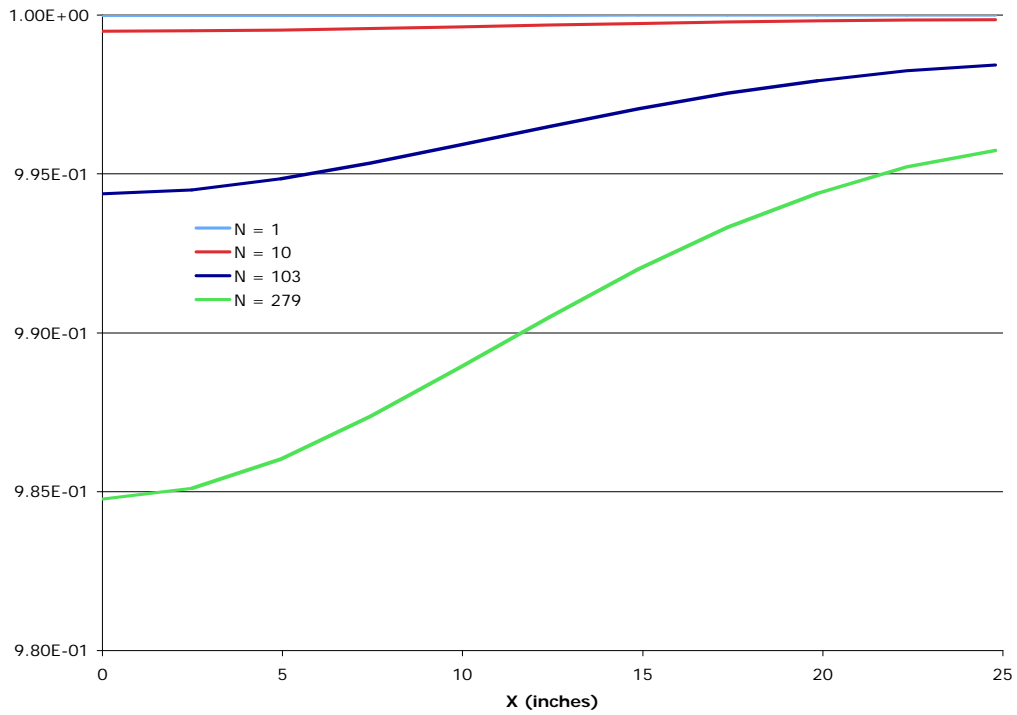


Figure 5.10: Distribution of residual stiffness along the transverse center of the mesh.

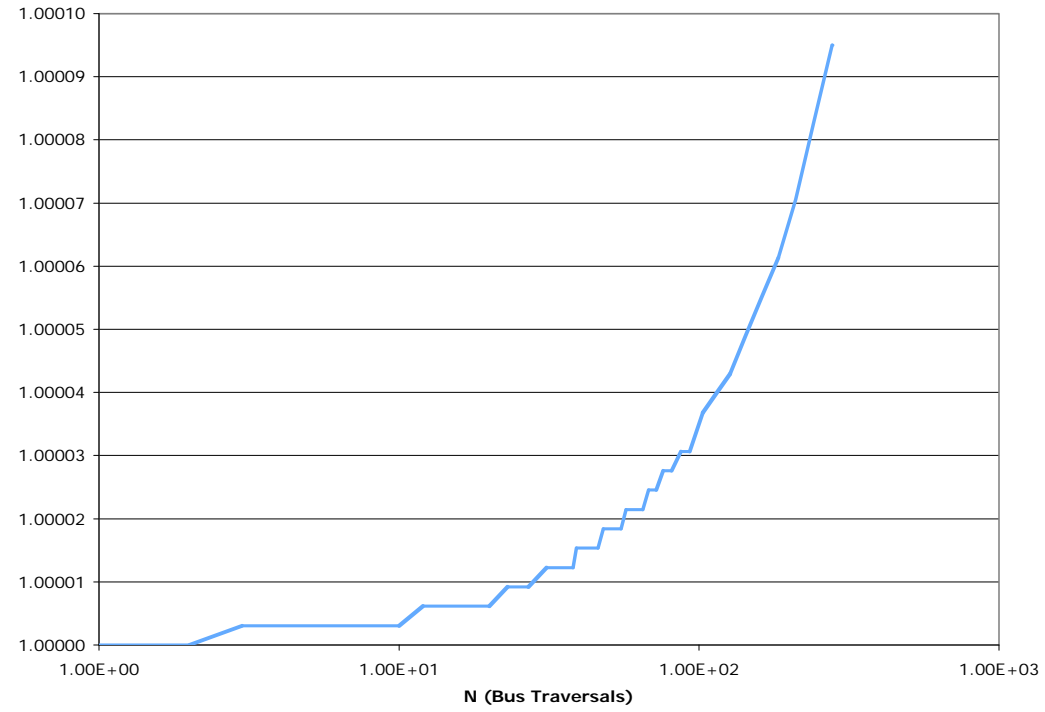


Figure 5.11: History of the (normalized) displacement under the front load.

CONCLUSION AND RECOMMENDATIONS

This report studies fatigue damage of three pavement structures: flexible (AC), rigid (PCC), and rigid beam. The third type refers to a pavement whose main structural elements are PCC beams located under the wheel paths. The analysis employs three-dimensional finite element models to represent the structures. The structures are subjected to a dead load due to self-weight, and to cyclic loading from articulated buses of the type employed by AC Transit. Each tire is represented as a moving circular pressure footprint with a uniform contact pressure of 110 psi.

A continuum damage mechanics model was developed to account for fatigue damage in the structural layers of the pavements. Additionally, a cycle-jump procedure was established in order to enable predicting fatigue due to high-cycle loading. This procedure avoids the use of an explicit function that describes the damage evolution as a function of the number of cycles.

Properties for the AR8000 AC material were determined by matching fatigue beam test results at four different strain levels. Good matches were obtained for the three higher levels of strain. At the lowest level, a good match is obtained up to about 120,000 cycles. At that point the model predicts a rapid deterioration, while actual test data shows that the tested specimen failed at about 3,000,000 cycles. It should be noted, however, that a very small change in the linear hardening of the threshold would cause the model to predict that the specimen would never fail. Alternatively, if the prescribed displacement were slightly reduced, then the model would predict an infinite fatigue life. Thus, the discrepancy between the model prediction and actual test results were deemed acceptable.

Unfortunately, no raw data was available for fatigue tests of PCC materials. The data reported in the literature summarizes the fatigue life as a function of stress ratio (applied stress normalized by the modulus of rupture). Therefore, the damage properties developed for AR8000 are used also for PCC, with the threshold properties reduced by a factor of ten in order to enable damage development. Due to this limitation the analyses of two structures employing PCC do not provide actual life prediction. Instead, they offer a performance comparison between the two structural systems. This information is very useful because, while there are established empirical procedures to determine the expected fatigue life for PCC pavements, no such procedures are available for pavements employing beams. Thus, the present work can bridge the knowledge gap in empirical procedures.

The simulation results show, for the PCC beam dimensions considered herein, a damage level that is roughly 6% larger than that observed for a corresponding number of cycles when a full PCC layer is employed. This finding should be used to obtain a life prediction based on an empirical design procedure. Alternatively, the thickness of the beam can be changed from 10 inches to about 10.25 inches in order to ensure that the two sections yield the same service life.

The simulations for the flexible pavements show an expected service life of about 500,000 bus traversals. This prediction is obtained by extrapolating the maximum damage observed in the pavement, and it falls short of the expected service life predicted by (validated) empirical procedures. On the other hand, if the prediction is based on extrapolating the change in deflection under the front tire, then a life expectancy of about 2,000,000 cycles is anticipated.

This latter prediction is in line with what can be expected based on empirical design. Thus, two lessons must be drawn from the results reported herein. First, while the simulations herein offer a realistic analysis, they do not account for all the nonlinear effects present in the actual system. Therefore, a comprehensive validation should be undertaken. Unfortunately, such a validation program cannot be accommodated within the limited scope of this study. Second, it is not possible to extrapolate directly from the maximum damage recorded to the service life of pavements. A better measure is offered by examining the deflection history, which offers a system evaluation rather than an evaluation of what takes place at a specific material point.

Recommendations for future work include:

- Enhance the damage threshold hardening law. As shown in Section 4, adding linear hardening of the damage threshold significantly improved the quality of the fit for low strain fatigue testing. This law should be enhanced in order to extend the range of the fit beyond the current level (about 120,000 cycles).
- Obtain damage properties for PCC. This task requires access to the raw data used to generate the fatigue transfer plots reported in the literature.
- Undertake simulations of rigid pavements (both slab and beam).²
- For both flexible and rigid pavements, develop calibration factors by comparing the simulation results with field experience. This effort is necessary in order to account for certain effects ignored in the analysis. For example, a uniform state of temperature was assumed herein. In reality, however, there is a variation in the temperature with thickness, which influences the development of fatigue distress.
- Consider the effect of thermal joints (PCC pavements). This aspect was ignored in the present study. A future study should examine the effect of load transfer (from one slab to the next) on fatigue life. Moreover, the effectiveness of including dowels should also be reviewed. For example, the study should consider if the presence of the OGAC layer negates the need for dowels.

² All future analyses should consider extending the loaded span, and reducing the interval between load steps (in order to attain a uniform state in the longitudinal direction).

REFERENCES

- Hughes, T.J.R., [1987], *The Finite Element Method, Linear Static and Dynamic Finite Element Analysis*, Prentice-Hall, Inc. Englewood Cliffs, New Jersey.
- Kohler, E., A. Ali, and J. Harvey, [2005], “Goal 4 Long Life Pavement Rehabilitation Strategies – Rigid: Flexural Fatigue Life of Hydraulic Cement Concrete Beams,” Partnered Pavement Research Center Report, University of California, Davis and Berkeley.
- Lemaitre, J., [1992], *A Course on Damage Mechanics*, Springer-Verlag, Berlin.
- Peerlings, R.H.J, W.A.M. Brekelmans, R. de Borst, and M.G.D. Geers, [2000], “Gradient-Enhanced Damage Modeling of High-Cycle Fatigue,” *International Journal for Numerical Methods in Engineering*, 49: 1547-1569.
- Wu, R., [2005], *Finite Element Analysis of Reflective Cracking in Asphalt Concrete Pavements*, Ph.D. dissertation, University of California, Berkeley.